L. Trainelli, M. Gennaretti, G. Bernardini, A. Rolando, C.E.D. Riboldi, M. Redaelli, L. Riviello, A. Scandroglio

Innovative Helicopter In-Flight Noise Monitoring Systems Enabled by Rotor-State Measurements

Noise Mapping, Vol. 3, N. 1, 2016, p. 190-215
doi:10.1515/noise-2016-0014

Research Article **Open Access**

Lorenzo Trainelli, Massimo Gennaretti, Giovanni Bernardini, Alberto Rolando, Carlo E. D. Riboldi, Matteo Redaelli, Luca Riviello, and Alessandro Scandroglio

Innovative Helicopter In-Flight Noise Monitoring Systems Enabled by Rotor-State Measurements

DOI 10.1515/noise-2016-0014
Received Nov 18, 2015; accepted May 18, 2016

Abstract: The present contribution aims at providing a comprehensive illustration of a new approach to rotorcraft noise abatement, especially during terminal procedures, when the vehicle approaches the ground and the acoustic impact is higher. This approach pursues the development of technologies and tools for real-time, in-flight monitoring of the emitted noise. The effect of the acoustic radiation is presented to the pilot in a condensed, practical form on a new cockpit instrumentation, the Pilot Acoustic Indicator (PAI), to be used for performing quieter maneuvers. The PAI is based on the synergetic composition of pre-calculated acoustic data, which are used in a noise estimation algorithm together with the data gathered by an innovative contactless measurement system, capable of acquiring the main rotor blade motion. The paper reports on the current studies in unsteady and quasi-steady aeroacoustic prediction and tip-path-plane angle of attack and thrust coefficient observation. Results on novel methodologies are discussed, together with the main features of the PAI design and development process.

List of Acronyms

ADC	Air Data Computer
BPF	Blade-Passage Frequency
BVI	Blade-Vortex Interaction
BVISPL	BVI-weighted SPL
EPN	Effective Perceived Noise
FMS	Flight Management System
GRC	Green RotorCraft
HMI	Human-Machine Interface
IRS	Inertial Reference System
ITD	Integrated Technology Demonstrator
JTI	Joint Technology Initiative
MFD	Multi-Function Display
OASPL	OverAll SPL
PAI	Pilot Acoustic Indicator
RSF	Rotor State Feedback
SPL	Sound Pressure Level
TCP/IP	Transmission Control Protocol/Internet Protocol
TPP	Tip-Path Plane
TPP-AOA	TPP Angle Of Attack
WP	Work Package

1 Motivation

Noise radiated upon populated areas is among the main factors that limit public acceptance of rotorcraft vehicles, hindering a wider diffusion of these machines, which are not only extremely useful, but basically irreplaceable in a number of tasks of high social relevance. Naturally, this problem is even more so felt when operating in proximity to the ground, as in approach and departure procedures. This impact is expected to grow as rotorcraft operations

Lorenzo Trainelli: Department of Aerospace Science and Technology, Politecnico di Milano, Milano, Italy; Email: lorenzo.trainelli@polimi.it
Massimo Gennaretti: Department of Engineering, Università Roma Tre, Roma, Italy; Email: massimo.gennaretti@uniroma3.it
Giovanni Bernardini: Department of Engineering, Università Roma Tre, Roma, Italy; Email: giovanni.bernardini@uniroma3.it
Alberto Rolando: Department of Aerospace Science and Technology, Politecnico di Milano, Milano, Italy; Email: alberto.rolando@polimi.it
Carlo E. D. Riboldi: Department of Aerospace Science and Technology, Politecnico di Milano, Milano, Italy; Email: carlo.riboldi@polimi.it
Matteo Redaelli: Leonardo – Finmeccanica Helicopter Division, Cascina Costa di Samarate, Italy; Email: matteo.redaelli@finmeccanica.com
Luca Riviello: Leonardo – Finmeccanica Helicopter Division, Cascina Costa di Samarate, Italy; Email: luca.riviello@finmeccanica.com
Alessandro Scandroglio: Leonardo – Finmeccanica Helicopter Division, Cascina Costa di Samarate, Italy; Email: alessandro.scandroglio@finmeccanica.com

to and from airports will increase, with helicopters following terminal routes designed for fixed wing aircraft. Therefore, important efforts are currently made towards the reduction of rotorcraft acoustic impact, both by helicopter manufacturers and by research institutes and academia. As helicopter noise is a complex effect generated aerodynamically, through the main and tail rotors, as well as mechanically, by the engine and transmission system, the directions of research include both topics in the design of inherently lower-noise vehicle and subsystem, and the definition of flight procedures that can effectively contain environmental pollution.

A significant number of works has been devoted in past years to helicopter noise reduction. Due to the complexity of the aerodynamic interactions involved in helicopter acoustics, and the difficulties in the estimation of emitted noise from on-board measurements [1–4], preliminary research efforts have suggested solutions able to reduce noise mainly by means of a suitable design of the rotor blades [5–8]. This approach has proven effective mainly under the operational conditions considered for blade design, whereas it is not effective in off-design conditions. Due to the relationship between blade flap oscillation and noise intensity, a reduction of the flapping excursion through harmonic control has been tried as a mean to reduce the emission intensity [9, 10]. This class of solutions, based on the application of a suitable pitch control action targeting prescribed harmonics in the blade displacement signal, does not bear completely successful results in term of noise containment, due to the fact that the noise intensity perceived on the ground is bound to the orientation of the helicopter and other flight mechanics parameters, besides depending on blade flap motion and blade aerodynamic characteristics.

More recent research efforts have shown that it is possible to effectively relate the noise intensity measured on the ground to three aero-mechanical parameters [11, 12]: the advance ratio, the thrust coefficient, and the tip-path-plane angle of attack. It has been shown that a database of emission intensities associated to a hemisphere surrounding the rotor can be parameterized with respect to these quantities when executing an approach maneuver with a prescribed profile [13–15].

Research activities connected to European Union-funded programs have also been actively targeting rotorcraft noise reduction, such as those carried out in the FRIENDCOPTER project of the 6th Framework Programme and within the development of the Green Rotorcraft (GRC) Integrated Technology Demonstrator (ITD) of the Clean Sky Joint Technology Initiative (JTI). The Clean Sky JTI, started in 2008 as a public-private partnership between the European Commission and the aeronautical industry, is the largest aeronautical research program ever launched in Europe seeking the development of innovative technologies aimed at reducing the environmental impact of air transport. The ambitious goals of the Clean Sky JTI are summarized by a reduction of CO_2 emissions by 50%, of NO_x emissions by 80% and of perceived noise by 50% within the year 2020. The Clean Sky JTI program is comprised of six Integrated Technology Demonstrators (ITDs), each of which pertains to a segment of civil air transport. Among these ITDs, the Green RotorCraft (GRC) is dedicated to the enhancement of rotary-wing vehicle environmental performance and sustainability, exploiting various technologies such as innovative rotor blades, airframe drag reduction, high compression engines, advanced electrical systems, and environmentally friendly flight paths. This is expected to provide a reduction in fuel consumption by 6%, and in perceived noise by 5 EPN (Effective Perceived Noise) dB.

Within the GRC, an important driver is represented by the will to derive solutions characterized by actual integratability within production helicopters, high cost-effectiveness in a short-medium term horizon, and by the possibility to apply these solutions to the wider possible amount of existing helicopter fleets. Therefore, the development of optimal low-noise trajectories is considered among the best possible solutions. In fact, by exploiting the rotorcraft intrinsic agility, radiated noise may effectively be contained by flying suitable procedures designed to take into account environmental pollution constraints. The resulting benefits may be substantially enhanced by the ability of the pilot to monitor acoustic emissions during flight, through dedicated real-time noise monitoring systems. To this end, the key elements are an off-line acoustic analysis based on numerical simulation to provide the necessary knowledge base, especially on aerodynamically generated emissions, and the development of innovative on board instrumentation enabling in-flight noise estimation.

2 The MANOEUVRES project

2.1 Concept

The MANOEUVRES (Manoeuvring Noise Evaluation Using Validated Rotor State Estimation Systems) project has been launched in response to the SP1-JTI-CS-2013-01 call [16] issued by the Clean Sky JTI. MANOEUVRES aims at demonstrating the feasibility of noise abatement in ro-

torcraft terminal maneuvers based on in-flight monitoring of the emitted noise, by delivering the related habilitating technologies. These are integrated within an innovative real-time noise estimation system designed in view of its industrial application on current and future production helicopters.

The MANOEUVRES in-flight noise estimation and monitoring system is conceived as follows. A new cockpit instrument, the Pilot Acoustic Indicator (PAI), provides real-time acoustic impact information to the pilot, based on a noise estimation algorithm which synthesizes a noise index from the calculation of the current Sound Pressure Level (SPL) distribution around the aircraft. Having an on-board instrument conveying information on the emitted noise footprint to the pilot would be advantageous for multiple reasons. First, the pilot could monitor the intensity and evolution of the helicopter acoustic emission in real time and apply, upon nearing noise thresholds, suitable corrective actions to keep it within acceptable limits. Also, such an instrument would allow the assessment of the noise impact of different manoeuvring strategies when designing and evaluating low-impact terminal procedures, without the need to fly at low altitudes over an *ad-hoc* prepared, ground-deployed acoustic acquisition infrastructure. Finally, it would permit pilot familiarization with noise impact connected to maneuvering flight, as well as a convenient self-evaluation tool in training activities connected to low-noise procedures.

The SPL distribution is interpolated among a database generated off-line for the present helicopter model, based on steady-state noise predictions. Relying on this kind of acoustic data is an unavoidable consequence of the computational costs related to unsteady noise predictions, which inhibit real-time applications to date. However, the limitations connected to the steady-state calculations can be overcome by employing real-time measurements to feed the noise database. In fact, the interpolation is driven by input parameters which are retrieved partly by the helicopter avionics, and partly by the outcomes of direct measurements of the kinematic state of the main rotor. These are made possible through a new sensor system capable of acquiring the current rotor blade motion.

Indeed, the differences between steady-state and unsteady predictions of the actual helicopter acoustic emission can be related to the variation of the blade loading and rotor disc orientation resulting in the two cases, for the same values of helicopter weight, airspeed and flight path angle. By estimating the current rotor thrust through acceleration measurements available on board and direct measuring rotor blade attitude, the current blade loading and rotor disc orientation can be determined, enabling the quasi-steady prediction based on the steady-state database.

2.2 Consortium and work structure

The MANOEUVRES project has been presented in [17, 18]. It is being carried out by a consortium involving four partners, in close co-operation with Leonardo – Finmeccanica Helicopter Division (FHD), a world-class European rotorcraft manufacturer. The consortium participants are two academic institutions, Politecnico di Milano and Università Roma Tre, and two companies, Logic Spa and Vicoter Snc. Politecnico di Milano contributes to the project through the commitment of personnel and facilities from the Department of Aerospace Science and Technology, the Department of Mechanical Engineering, and the Department of Electronics, Information and Bioengineering. This involvement provides solid capabilities in modelling, design, simulation and testing of aeromechanical systems, including rotorcraft; measurement system modelling, design and testing; experimental data acquisition and processing; control system design and simulation. Università Roma Tre contributes through the commitment of personnel and facilities from the Department of Engineering, with a long-standing expertise in rotorcraft aerodynamic and aeroacoustic prediction and analysis. Logic is a leading avionics company, specialized in the design, development and production of avionics equipment and systems for several production airplanes and helicopters. Its contribution focuses on requirement definition for the innovative rotor sensor system and the pilot graphical interface. Finally, Vicoter is a small engineering company with a strong background in mechanical, structural and acoustic testing and data processing, including design and verification of experimental rigs for testing of aerospace systems.

This team is currently developing a 32-month, highly multidisciplinary work program scheduled to end in May, 2016. The program activities, according to the above concept description, mainly involve aeroacoustic numerical studies, rotor state measurement techniques, real-time noise estimation techniques and on board instrumentation. These diverse topics are integrated within a technical implementation comprised of four Work Packages (WPs). WP1 is dedicated to rotorcraft aeroacoustic prediction, including the generation of the steady-state database of acoustic hemispheres, the development of a fully unsteady simulation tool for arbitrary maneuvering flight conditions, and a wealth of analyses to study the correlation between steady and unsteady results, the assessment

of the accuracy of fully unsteady estimations compared to flight test data, and the evaluation of the sensitivity of numerical predictions to perturbations in the flown trajectory. The sequence of WP2 and WP3 addresses the development of the novel rotor state measurement system. Relevant activities consist of a thorough technology selection process, followed by a competitive preliminary development of multiple candidate solutions (WP2), which leads to the choice of the definitive system to be implemented and integrated onboard an actual helicopter for a final demonstration (WP3). Finally, Work Package 4 (WP4) is devoted to the development of the in-flight noise monitoring system, based on the formulation of the noise estimation algorithm and on the development of the PAI human-machine interface (HMI), including design, implementation and testing.

2.3 Rotor state measurement system

In the MANOEUVRES project, a great effort is committed to the development of an innovative rotor state measurement system able to capture the rotor disc orientation by sensing the rotor blade angles with respect to the hub. This system is conceived for swift integration on board current production helicopters, departing from the configurations based on mechanical probing typically employed in experimental applications, such as Leonardo–FHD's MOVPAL [19]. To this end, a complete set of requirements concerning not only the system's performance, functionality and safety, but also environmental resistance, reliability, testability and maintainability have been considered. A first stage analysis considered a wide range of possible technologies, envisaging their possible application with transducers located either on the fuselage, or on the main rotor head. All contemplated concepts implement contactless measurement techniques, in an effort to maximize the system reliability, endurance, and applicability to diverse rotorcraft vehicles.

Subsequently, on the basis of expected metrological performance, as well as installation and environmental requirements, general regulations, flight standards and design guidelines, three candidate solutions, all mounted on the main rotor head, have been selected. These concepts have been integrated in full-scale prototypes and thoroughly tested on a variety of experimental rigs, including a specially equipped, electrically actuated Agusta A109MKII ironbird at the Politecnico di Milano laboratories and the AW139 hub endurance rig made available by Leonardo – FHD at its Cascina Costa premises. Test campaigns performed on these rigs allowed to assess the measurement system capabilities in simplified conditions, tackling measurement accuracy, functionality under representative vibration and rotation conditions, as well as with respect to fully coupled flap, pitch and lead/lag motions as found in operational flight conditions. This extensive test campaign has led to promising results for all three solutions, which have been ranked in a final list, from which the best option has been picked for final implementation.

This final phase involves the bringing to maturity of the selected solution. This system, complete with proper signal processing procedures and adequate mechanical, power and communication interfaces, at the moment of writing is further developed and tested, towards the integration onboard an AgustaWestland helicopter. A test campaign of this integrated system will allow the final demonstration of its functional characteristics and performance. An assessment through a comparison with an existing experimental measurement system will be carried out. Only ground tests were targeted from the start of the project, but a dedicated flight test campaign has been eventually performed, to achieve an even more representative demonstration. The full design and development work for the rotor state measurement system is addressed in [20].

2.4 Innovative flight control laws

The availability of a rotor state measurement system makes it all too natural to investigate the possible advantages achievable by applying a Rotor State Feedback (RSF) approach to the design of innovative flight control laws, in addition to the feedback based on traditional fuselage attitude and angular rate measurements. These laws are aimed to improve pilot/vehicle capabilities, reducing pilot workload thanks to enhanced noise rejection properties, while retaining adequate levels of robustness and fault tolerance. Within the WP3 and WP3 of the MANOEUVRES project, significant resources have been allocated to the study of RSF applications enabled by the collective and cyclic flapping measurements made available by the rotor state measurement system, in order to evaluate the benefits that can be achieved. A successful control system design and synthesis activity has been performed, as reported in [21–23].

2.5 On the present paper

The present paper is devoted to reporting on the main activities carried out within the WP1 and WP4 of the MA-

NOEUVRES project. In particular, we address: (i) studies in unsteady maneuvering rotorcraft acoustic prediction; (ii) a novel observation methodology to estimate the main rotor thrust coefficient and the angle of attack of the main rotor tip-path plane (TPP), or TPP-AOA, which are not directly measurable on board a typical helicopter; and (iii) the development of a real-time noise monitoring methodology, from the noise estimation computational procedure to the PAI design and development.

Section 3 illustrates the methodology for acoustic prediction, and provides the comparison of results obtained through three different numerical approaches, one based on a fully unsteady computation and the others based on a quasi-steady formulation. This work has been presented, with additional details, in [24]. Section 4 is devoted to the observation methodology developed for the real-time estimation of the parameters that convey blade loading and rotor disc orientation information needed for the estimation of the acoustic emission. Also this work has been presented, with additional details, in [25]. Section 5 describes the noise monitoring system, which is the subject of a dedicated presentation found in [26].

3 Acoustic prediction

3.1 Steady-state acoustic analysis

Among the several strategies examined for noise alleviation purposes, in the last decade, the identification of minimum-noise, optimal trajectories has been widely applied, in that providing effective solutions without requiring specific machine adaptation (*i.e.* re-design or retrofit solutions). This methodology often combines a flight simulation model, a near-field noise emission model, a far-field noise propagation model and geographic information to make optimization suitable for the orography and population density distribution of the interested area. Identified minimum noise trajectories might correspond to unsteady maneuvers including turns, varying flight-path slope, accelerations and decelerations, which require acoustic source model updating, accordingly to the change in flight conditions.

In order to avoid numerically expensive acoustic predictions, the source model update is usually accomplished by deriving the near-field model, provided in terms of a hemispheric acoustic map rigidly connected to the rotorcraft, as seen in Figure 1, extracted from an appropriate database. In such a quasi-steady acoustic approach, the database is generated through off-line aeroacoustic analysis of rectilinear steady-state flight conditions, within a given domain of flight parameters suitably characterizing the noise source state (for related research work, see [27–31], as well as [32], which has been experimentally validated through flight testing, [1, 4]). The database is typically parameterized in terms of the helicopter advance ratio μ, the main rotor thrust coefficient C_T, and the main rotor TPP-AOA α_{TPP}. Similar aeroacoustic information was required as input in the WP4 of the MANOEUVRES project, as the PAI relies on a noise estimation algorithm which determines in real-time a suitable measure of the acoustic impact by interpolating the hemispheric acoustic map within the database, as a function of current values of (μ, C_T, α_{TPP}). Results related to the application of this approach are given in [13–15].

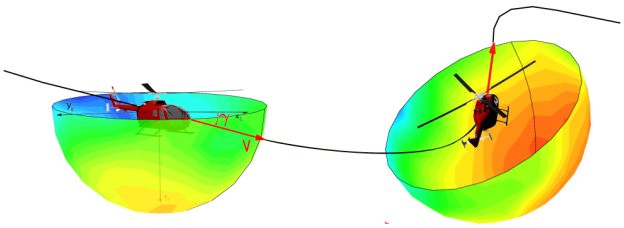

Figure 1: Noise hemisphere concept.

3.2 Methods for unsteady acoustic analysis

In the MANOEUVRES project, the above mentioned quasi-steady approach is developed in two different variations, suitable for real-time on board applications. Also, a fully unsteady approach is developed, in order to provide a highly accurate solution for arbitrary motion conditions. With such tools at hand, the work currently ongoing pursues a twofold goal:

i The assessment of the accuracy of noise predictions based on quasi-steady acoustic approaches with respect to those given by fully unsteady simulations;
ii The analysis of sensitivity of quasi-steady acoustic predictions on the accuracy of the estimation of the three parameters (μ, C_T, α_{TPP}) used to extract the current instantaneous hemispheric acoustic map from the database.

The noise prediction techniques examined in this paper are termed Techniques A, B and C. Technique A is based on a fully unsteady approach, where all flight data, including pilot controls, helicopter attitude, rotor states and airloads, are provided by a rotorcraft aeromechanics

simulation code coupled with a full-unstructured panel method solution tool for rotor aerodynamics. Once spanwise distributed airloads are known, a compact-source aeroacoustic solver based on the Farassat Formulation 1A [33, 34] is applied to determine the time history of the corresponding acoustic hemispheres, as evaluated by appropriate signal windowing. Techniques B and C share a common framework, as they are both based on the quasi-steady approach using a pre-calculated acoustic database. In Technique C, a simplified aeromechanical model of the rotorcraft is used to derive real-time estimates of the three parameters (μ, C_T, α_{TPP}), while in Technique B the model-based estimation of the TPP-AOA is replaced by an evaluation process that exploits the observation methodology described in Section 4, which in turn takes advantage of the availability of the MANOEUVRES rotor state measurement system. Technique B is thus applicable in flight to feed the PAI, while Technique C represents a possible methodology that could be applied without building on the MANOEUVRES developments.

From the previous description, a comparison between the predictions provided by Techniques B and C highlights the sensitivity of quasi-steady simulations on the accuracy of rotor TPP-AOA evaluation. On the other hand, comparing Techniques A and B, or A and C, provides a measure of the suitability of quasi-steady approaches in approximating transient solutions. At the moment of writing, a further action in assessing the accuracy of the fully unsteady approach is being performed through a correlation between numerical predictions and experimental data gathered in a GRC5 flight test campaign performed in October 2014 with an instrumented AgustaWestland AW139 flying over an area equipped with 31 ground microphones for acoustic measurements.

The three techniques outlined above require the sequential application of three solution tools:

1. An aeromechanic solver for the identification of the helicopter flight conditions corresponding to a given maneuver;
2. A rotor aerodynamics solver that, for given flight conditions provides the associated blade airloads;
3. An aeroacoustic prediction tool that determines the acoustic field generated by the rotor loads.

These tools are applied either to study as accurately as possible the noise emitted during an unsteady maneuver of the helicopter, or to generate a database of noise sources corresponding to a number of rectilinear, steady-flight conditions to be exploited in the quasi-steady acoustic approaches. The noise sources are given in terms of SPL evaluated on a hemispheric surface centred at the main rotor hub, fixed with the fuselage and with the equatorial plane parallel to the cabin floor. The aeroacoustics, aeromechanics and aerodynamics prediction tools applied in this work are described in the next paragraphs.

3.3 Aeroacoustic solver

Noise radiated by helicopter rotor blades is evaluated through the widely-used, computationally efficient boundary integral Formulation 1A of Farassat [34], which solves the Ffowcs Williams and Hawkings' equation. When the velocity of the rotor blades is far from the transonic/supersonic range, this formulation yields the aeroacoustic field as a superposition of two terms, both expressed by integrals evaluated over the actual blade surface, S_B: the loading noise, p'_L, related to the distribution of pressure over blade surfaces,

$$\begin{aligned} 4\pi p'_L(\mathbf{x},t) = {} & \frac{1}{c_0}\int_{S_B}\left[\frac{\dot{\tilde{p}}\mathbf{n}\cdot\hat{\mathbf{r}}+\tilde{p}\dot{\mathbf{n}}\cdot\hat{\mathbf{r}}}{r|1-M_r|^2}\right]_\tau dS(\mathbf{y}) \\ & + \int_{S_B}\left[\frac{\tilde{p}\mathbf{n}\cdot\hat{\mathbf{r}}-\tilde{p}\mathbf{M}\cdot\mathbf{n}}{r^2|1-M_r|^2}\right]_\tau dS(\mathbf{y}) \\ & + \frac{1}{c_0}\int_{S_B}\left[\frac{\tilde{p}\mathbf{n}\cdot\hat{\mathbf{r}}}{r^2|1-M_r|^3}r\dot{\mathbf{M}}\cdot\hat{\mathbf{r}}\right]_\tau dS(\mathbf{y}) \\ & + \int_{S_B}\left[\frac{\tilde{p}\mathbf{n}\cdot\hat{\mathbf{r}}}{r^2|1-M_r|^3}\left(M_r-M^2\right)\right]_\tau dS(\mathbf{y}) \end{aligned} \tag{1}$$

and the thickness noise, p'_T, that depends on blade geometry and kinematics,

$$\begin{aligned} 4\pi p'_T(\mathbf{x},t) = {} & \int_{S_B}\left[\frac{\rho_0\dot{v}_n}{r|1-M_r|^2}\right]_\tau dS(\mathbf{y}) \\ & + \int_{S_B}\left[\frac{\rho_0 v_n\left(r\dot{\mathbf{M}}\cdot\hat{\mathbf{r}}+c_0\left(M_r-M^2\right)\right)}{r^2|1-M_r|^3}\right]_\tau dS(\mathbf{y}) \end{aligned} \tag{2}$$

In the equation above, $\mathbf{r} = \mathbf{x} - \mathbf{y}$ denotes the distance vector between the observer position $\mathbf{x}$ and the source position $\mathbf{y}$, whereas $r = \|\mathbf{r}\|$ and $\hat{\mathbf{r}} = \mathbf{r}/r$ is the unit vector along the source-observer direction. In addition, c_0 and ρ_0 are the speed of sound and the density in the undisturbed medium, respectively, $\tilde{p} = (p - p_0)$ is the differential pressure, with p representing local pressure at the source location and p_0 the pressure in the undisturbed medium, $\mathbf{M} = \mathbf{v}_B/c_0$ is the local Mach vector with $\mathbf{v}_B$ the local blade velocity and $M = \|\mathbf{M}\|$ the local Mach number, $M_r = \mathbf{M}\cdot\hat{\mathbf{r}}$, and $v_n = \mathbf{v}_B\cdot\mathbf{n}$, where $\mathbf{n}$ is the outward blade surface unit normal vector. Superposed dots denote time derivatives observed in a frame of reference fixed with the

undisturbed medium. The notation $[\dots]_\tau$ indicates that all quantities within the brackets are evaluated at the emission time τ, *i.e.* the time at which the signal arriving in $\mathbf{x}$ at time t started from $\mathbf{y} \in S_B$ [34].

Leaving out applications in which high blade tip speed may engender transonic effects, in problems dealing with weakly loaded rotors, thickness and loading noise are of comparable magnitude (but different directivity), while for rotors that are strongly loaded and/or subject to impulsive load changes, thickness noise contribution tends to be negligible and the acoustic disturbance is dominated by loading noise. Rotors in blade-vortex interaction (BVI) conditions fall within this category of acoustic phenomena. Thus, from Eq. (1) it is apparent that for accurate noise simulation, accurate simulation of blade airloads is required.

Commonly, applications of aeroacoustic formulations for helicopter rotor analysis consider steady, rectilinear, trimmed flights. In these operative conditions both kinematics and aerodynamics are periodic thus yielding, correspondingly, periodic integrand functions, periodic kernels and, for observers rigidly connected to a helicopter-fixed frame of reference, periodic delays as well (it is worth noting that the periodicity occurs in coordinated turns). Differently, during unsteady helicopter maneuvers, kinematic and aerodynamic terms are non-periodic, thus increasing the complexity of the algorithms to be applied for implementing Eqs. (1) and (2). Emission time, τ, appearing in thickness and loading noise expressions is obtained by a root-finding problem for the following nonlinear equation,

$$\|\mathbf{x}(t) - \mathbf{y}(\tau)\| = c_0 (t - \tau) \tag{3}$$

and thus, the prediction of radiated noise requires the knowledge of the past time histories of blade pressure loads and vehicle and blade kinematics, for a time interval length depending on observer location. Indeed, the time histories of center of mass trajectory and velocity, vehicle attitude and angular velocity are necessary data to evaluate instantaneous values of kernels and integral coefficients of the discretized versions of Eqs. (1) and (2).

In order to optimize the computational performance of the aeroacoustic prediction tool, while limiting, at the same time, the amount of data exchange from aerodynamic to aeroacoustic solvers (a particularly relevant issue in noise predictions concerning rotorcraft manoeuvring flights), the so-called 'compact source' versions of it can be conveniently applied. Those introduced in the last decade are based on the knowledge of spanwise distribution of sectional lift [33, 35]. They provide satisfactorily accurate noise predictions when pressure distribution presents limited values of chordwise gradient, and are applicable by using blade loads predicted by aerodynamic models typically considered in rotorcraft comprehensive codes [36].

Starting from the Farassat 1A Formulation, the compact form of the loading noise term p'_L reads [33]

$$\begin{aligned} 4\pi p'_L(\mathbf{x}, t) = {} & \frac{1}{c_0} \int_0^R \left[\frac{\dot{\mathbf{L}} \cdot \hat{\mathbf{r}}}{r|1 - M_r|^2} \right]_\tau dl(\mathbf{y}) \\ & + \int_0^R \left[\frac{\mathbf{L} \cdot (\hat{\mathbf{r}} - \mathbf{M})}{r^2|1 - M_r|^2} \right]_\tau dl(\mathbf{y}) \\ & + \frac{1}{c_0} \int_0^R \left[\frac{\mathbf{L} \cdot \hat{\mathbf{r}} \left(r\dot{\mathbf{M}} \cdot \hat{\mathbf{r}} + c_0 \left(M_r - M^2 \right) \right)}{r^2|1 - M_r|^3} \right]_\tau dl(\mathbf{y}) \end{aligned} \tag{4}$$

where R is the blade radius and, in this case, $\mathbf{r} = \mathbf{x} - \mathbf{y}$ denotes the distance between the observer point $\mathbf{x}$ and the compacted source point $\mathbf{y}$ located along the blade span. In addition,

$$\mathbf{L} = -\int_{TE}^{LE} \Delta p \, \mathbf{n} \, ds \tag{5}$$

is the section force vector, with $\mathbf{n}$ and Δp denoting upward unit normal to airfoil mean-line and pressure jump, respectively. The compact-source integral representation in Eq. (4) is applicable when the chord length is negligible with respect to the source-observer distance r, and predicts the same radiated sound for any chordwise pressure distributions providing the same spanwise distribution of sectional forces $\mathbf{L}$. Preliminary results concerning this approach applied to rotorcraft maneuvering flight are given in [13–15].

3.4 Aeromechanic and aerodynamic simulation

Within project MANOEUVRES, the required aeromechanic and aerodynamic analyses are provided by Leonardo–FHD, making use of its reference company tools for flight dynamics and aerodynamics simulation, applied to accurate and reliable models of the AW139 based on past extensive validations. In particular, the commercial software Flightlab® by Advanced Rotorcraft Technology Inc. has been employed for the aeromechanic solution of all considered flight conditions, from the simple trim calculation to the unsteady simulation of entire flight procedures. This is a leading commercial software tool for rotorcraft modeling and analysis, widely applied by helicopter manufacturers, research centers and academia (see, *e.g.* [37–39]).

Whenever applicable, the flight mechanics simulation of unsteady flight is performed using a "maneuver tracking" technique, as described in [40]: similarly to what a pilot would do with the actual vehicle, a set of synthetic autopilot control logics is applied to steer the vehicle virtual model along the desired flight path, either coming from flight tests or designed for the purpose of the prediction tasks. The results of the aeromechanic simulation are used as inputs to the aerodynamic solver.

The aerodynamic simulation is determined by matching the pilot controls, the vehicle flight mechanics states and the main and tail rotor hub generalized forces – and therefore the parameters (μ, C_T, α_{TPP}) – as previously calculated in the flight dynamics analysis phase. This provides the aerodynamic blade loading required by the aeroacoustic solver described above. The tool used to this end is the Leonardo–FHD in-house ADPANEL solver. This is a full-unstructured panel code implementing the most advanced aerodynamic features in the field of potential methods. It is capable to represent body surfaces in unstructured-hybrid meshes, while the wake representation is based on the Constant Vorticity Contour modelling of both rotary and fixed wing (see, for instance [41]). Within this work, a fully coupled main rotor and tail rotor simulation is applied in order to take into account the interactions between the main rotor wake with the tail rotor blades. Based on Leonardo–FHD experience, this type of aerodynamic simulation is the most reliable for acoustic predictions.

While for Technique B, the TPP-AOA is retrieved by the aeromechanic simulations, as μ and C_T, in Technique C this parameter is evaluated through a simplified flight mechanics model for the helicopter, based on the conservation of linear momentum for a point mass. The TPP-AOA evaluation is then derived by the estimation of fuselage angle of attack and the main rotor longitudinal flapping corresponding to trimmed flight conditions, including the effects of load factor, when appropriate. This procedure is detailed in Section 5. On this basis, Technique C simulates the outcome of an on-board 'ideal' derivation using flight parameters and weight estimates augmented by the measurement of the helicopter acceleration vector via an inertial unit. Technique B, on the other hand, retrieves the full parameter array (μ, C_T, α_{TPP}) from an algebraic manipulation of the results of the aeromechanic prediction tool. In this way, Technique B represents what could be achieved from the application of the MANOEUVRES concept, where a direct measurement of main rotor blade motion provided by the rotor state measurement system yields an evaluation of longitudinal and lateral flapping angles. This, coupled with either a direct measurement (typically, via a swivelling air data boom) or the runtime observation method described in Section 4, would provide a value for the current TPP-AOA. Further details on the full array of the aeromechanic and aerodynamic simulation tools employed in this activity are found in [24].

3.5 Numerical results

The acoustic simulation techniques considered in this work are assessed through application to the prediction of noise emitted by the AgustaWestland AW139 helicopter during an approach maneuver. The AW139 is a 15-seat, intermediate-class, twin-engine helicopter, with a 5-blade fully-articulated main rotor of radius $R = 6.9$ m, a 4-blade tail rotor, and maximum take-off weight of 7000 kg_f. Although the complete helicopter has been considered in the aeromechanic and aerodynamic simulation, the attention here is focussed on the acoustic disturbance radiated by the main rotor only. Currently ongoing work considers also the contribution of the tail rotor.

Unsteady flight conditions corresponding to several approach procedures were considered. In particular, results from the analysis of procedure ID8021 are shown here, which is a maneuver starting from a level, steady rectilinear flight at 90 kn, followed by a 40 s uniform deceleration to 50 kn, a –9 deg slope steady descent flight, and ending with the transition to a final level, steady rectilinear flight. Figures 2–4 depict the evolution of the quantities (μ, C_T, α_{TPP}), as determined by the aeromechanics tool for the maneuver at hand. The corresponding flight-path angle is presented – without comma in Figure 5, whereas Figure 6 shows the associated main rotor blade pitch controls. In Figure 3 the TPP-AOA determined by the estimation process applied in Technique C is compared to that used in Technique B, evaluated by the aeromechanics tool: the discrepancy between the two curves presented in this

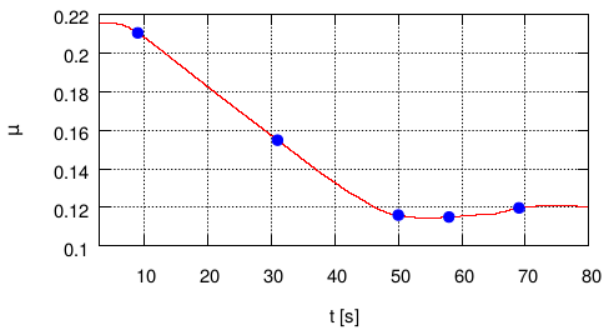

Figure 2: Advance ratio time history in maneuver ID8021.

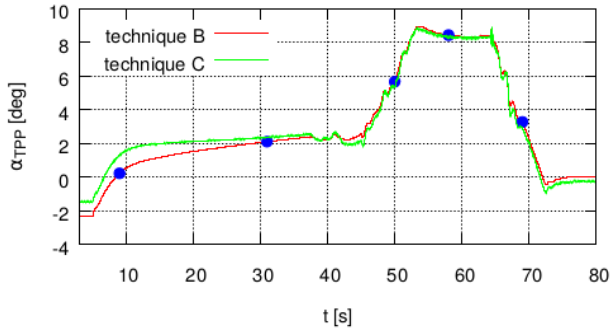

Figure 3: Main rotor TPP-AOA time history in maneuver ID8021.

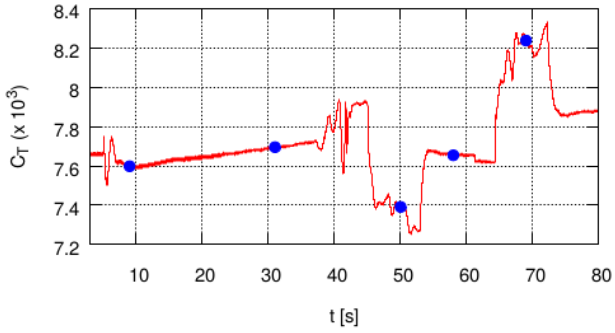

Figure 4: Thrust coefficient time history in maneuver ID8021.

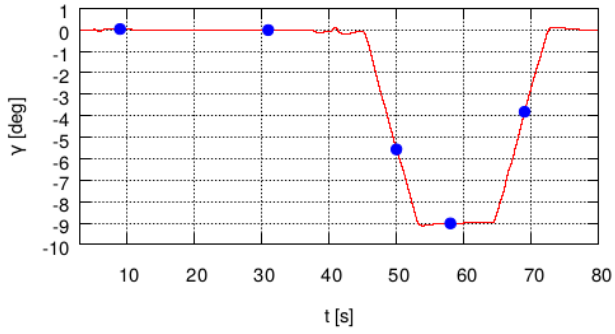

Figure 5: Flight-path angle time history in maneuver ID8021.

figure provides a first assessment of the advantages given by the direct measurement of blade flapping. In particular, a significant deviation is observed at the first control point, where the transition from uniform level flight to decelerated flight produces significant unsteady effects.

In each figure, five points along the time histories are marked: these represent flight conditions where different unsteady effects influence the noise emission, and thus seem to be appropriate to assess the capability of the quasi-steady approaches to predict helicopter acoustic disturbance during an arbitrary maneuver. At Point 1 (at about $t = 9$ s), the helicopter is at the end of the transition from the steady level flight to the uniformly decelerated flight, with noise affected by unsteady effects mainly

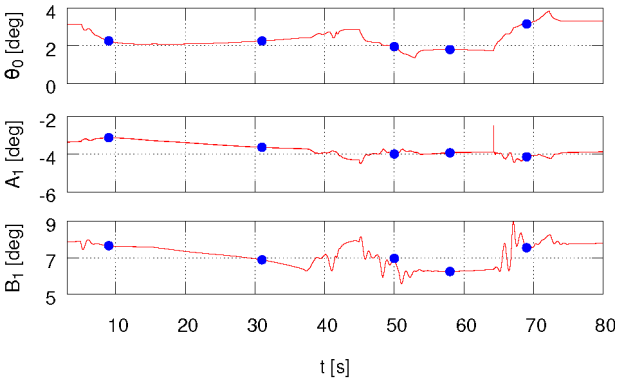

Figure 6: Collective and cyclic control time histories in maneuver ID8021.

through the corresponding TPP-AOA variation. At Point 2 (at about $t = 31$ s), the helicopter is in uniform decelerated flight, with inertial loads still affecting the TPP-AOA. Point 3 (at about $t = 50$ s) is located in the middle of the conversion phase from level to descending flight, where noise is mainly influenced by the unsteady effects due to the trajectory curvature, with a reduced value of the thrust coefficient. At Point 4 (at about $t = 58$ s) the helicopter is in uniform, rectilinear, descending flight, *i.e.* an operational condition characterized by high sensitivity of the acoustic response to the value of the TPP-AOA. Finally, at Point 5 (at about $t = 69$ s) the helicopter is maneuvering to restore level flight, and thus the emitted noise is strongly affected by inertial effects on rotor disk loads, with an increased value of the thrust coefficient.

In the following, the acoustic emissions provided by Technique A are compared with those estimated by Techniques B and C. Results from Technique A are obtained by suitably windowing the emitted noise until the vehicle reaches the considered control point, similarly to what is done by devices for noise measurement. This introduces an unavoidable, small time shift between unsteady and quasi-steady predictions (which are of instantaneous nature).

The evaluation is performed on a portion of a sphere of radius $r = 150$ m that surrounds the helicopter, having the equatorial plane parallel to the cabin floor. Specifically, the considered portion of the spherical surface is included in the domain defined by azimuthal angle (longitude) $\psi \in [0°, 360°]$ and polar angle (latitude) $\theta \in [0°, 120°]$. In the following, we shall refer to this surface as a 'hemisphere', for the sake of brevity, although it is clearly wider, as it comprises a 30° spherical band above the equatorial circle (this is made in view of the hemisphere spatial rotation before radiation to the ground, see Section 5). For the sake of clarity, the noise contour plots are provided in the mapped

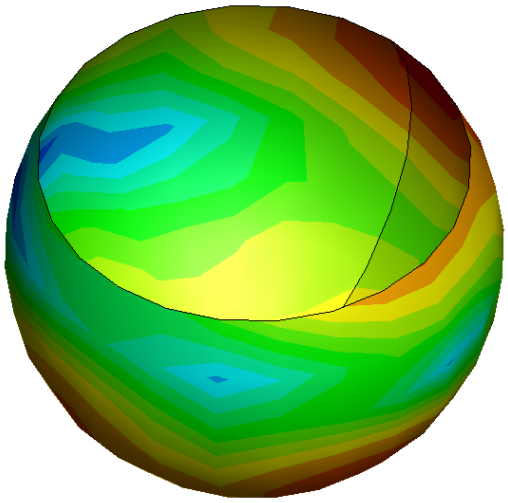

Figure 7: Three-dimensional representation of OASPL evaluated on the hemisphere surface by Technique A at point 1 in maneuver ID8021.

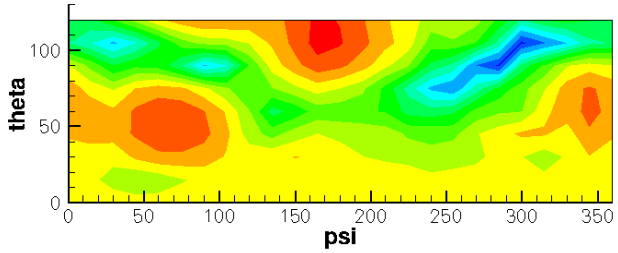

Figure 8: Two-dimensional representation of OASPL evaluated on the hemisphere surface by Technique A at point 1 in maneuver ID8021.

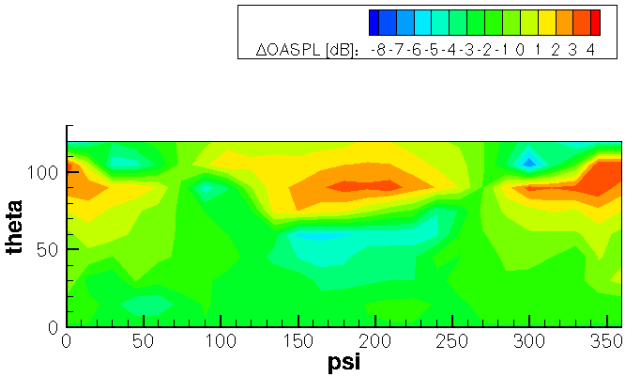

Figure 9: Technique A – B differential OASPL at point 1 in maneuver ID8021.

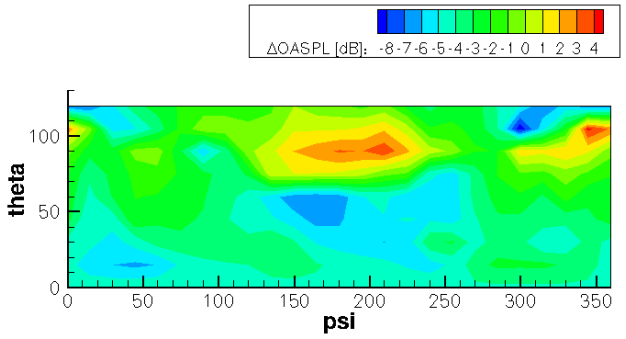

Figure 10: Technique A – C differential OASPL at point 1in maneuver ID8021.

coordinate plane (ψ, θ), with the ψ =180° meridian line located forward, ψ = 90° denoting starboard side, θ = 90° representing the equatorial parallel, whereas θ = 0° corresponds to the pole located underneath the helicopter.

In order to better understand the relation between the distribution of noise on the hemisphere and its two-dimensional representation, Figures 7 and 8 show the Overall Sound Pressure Level (OASPL) evaluated on the hemisphere at Point 1, respectively through a three-dimensional contour plot view and the corresponding view on the plane (ψ, θ). The colour scale is such that low-noise regions are blue, whereas high-noise regions are red, with a 2 dB colour variation increment.

At Point 1, where significant discrepancies between the TPP-AOA value used in Technique B and C appear, Figures 9 and 10 show the difference between the OASPL evaluated by Technique A and those predicted by Techniques B and C, respectively. First of all, it is possible to observe that both techniques based on the steady-state acoustic database provide a good estimation of the emitted noise on a large portion of the hemisphere, with some underestimation (red areas) or overestimation (blue areas) of the acoustic disturbance appearing in a few regions of limited extension. Furthermore, the comparison of Figures 9 and 10 reveals that Technique B yields predictions closer to those provided by Technique A than Technique C (except for a limited hemisphere region across the equatorial circle), thus demonstrating the advantages that are achievable in determining the TPP-AOA from direct rotor state measurements. However, the comparisons presented in terms of the OASPL evaluated for the noise frequency range included between the 6th BPF (Blade-Passage Frequency) and the 40th BPF are even more interesting. Indeed, this noise measure takes into account the most annoying acoustic effects related to BVI phenomena, and for this reason it is commonly named BVISPL.

Figures 11 and 12 depict the differential BVISPL contour plots between results given by Techniques A and B, and Techniques A and C, respectively. Akin to the OASPL analysis, BVISPL is satisfactorily predicted by quasi-steady approaches at a large part of the examined surface, with significant overestimation and underestima-

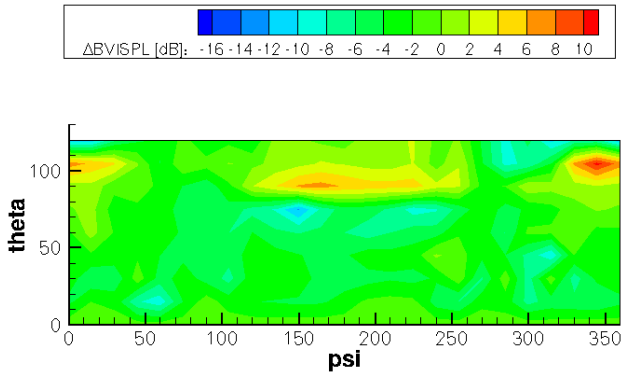

Figure 11: Technique A – B differential BVISPL at point 1 in maneuver ID8021.

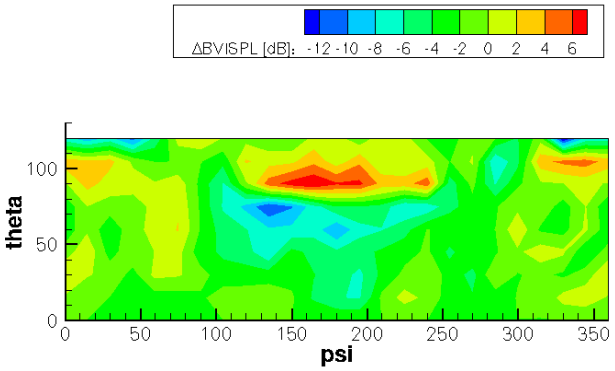

Figure 13: Technique A – B differential BVISPL at point 2 in maneuver ID8021.

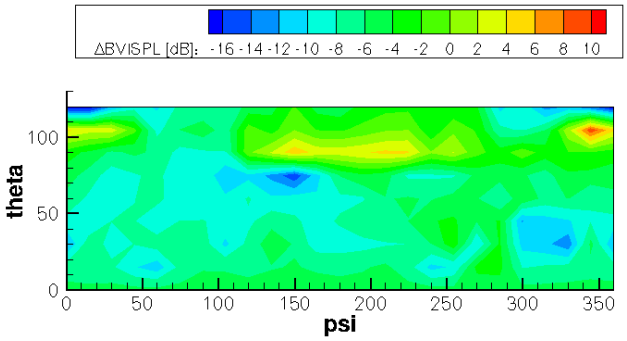

Figure 12: Technique A – C differential BVISPL at point 1 in maneuver ID8021.

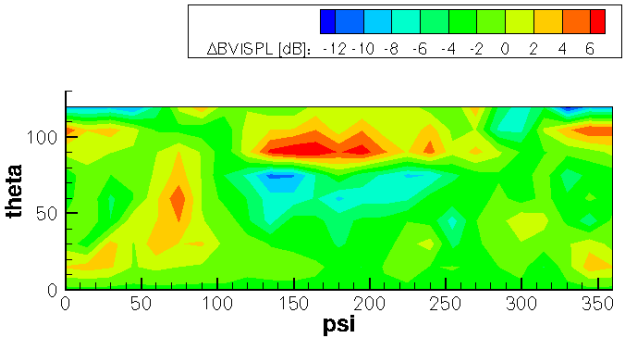

Figure 14: Technique A – C differential BVISPL at point 2 in maneuver ID8021.

tion limited to regions of small area. Likewise, the comparison of the quality of predictions from Techniques B and C proves the beneficial effects of the availability of accurate estimation of the TPP-AOA, with the former clearly closer to Technique A simulations, except for a very small area in the equatorial region. This is an important result, as it provides the PAI a suitable estimation to make the pilot aware of the acoustic annoyance produced by the helicopter maneuver.

At Point 2, unsteady effects are reduced with respect to Point 1, and this yields peaks of underestimation/overestimation of BVISPL predicted by Techniques B and C of lower intensity, as shown in Figs. 13 and 14. Likewise Point 1, predictions from Technique B are fairly more accurate than from Technique C, particularly in the region below the equatorial zone, which is that more related with the ground radiated noise.

At Point 3, the dominating effect is the alleviation of the C_T value due to the load factor reduction induced by the curvature of the trajectory. As depicted in Figure 4, the TPP-AOA values for Techniques B and C are almost identical and, therefore, the noise hemispheres extracted from the database by the two techniques are very similar. As a result, the BVISPL distributions (and OASPL as well) predicted by Techniques B and C are very close, both in terms of intensity and directivity, as proven by Figures 15 and 16 through comparison with Technique A. Akin to the previous points examined, some overestimation/underestimation of noise is present in the equatorial region.

At Point 4, as expected, Techniques A and B are in good agreement, particularly, in terms of the OASPL distribution which tends to hide the small unsteady effects still present at this trajectory point, as shown in Figure 17. Also, as inferred from Figure 4, predictions from Technique B and C are very close, even in terms of BVISPL, as seen in Figure 18 that presents the contour plot of the differences between the outcomes of Techniques B and C.

At Point 5, the inertial effects are of the same nature of those at Point 3, but of opposite sign, with the trajectory curvature inducing an increase of disk loading. Similarly, acoustic predictions from Techniques B and C are almost identical and of the same quality of those at Point 3. This is an expected outcome, considering that here the influence of inertial effects is much higher on C_T than on α_{TPP}, and observing that the TPP-AOA from Techniques B and C are

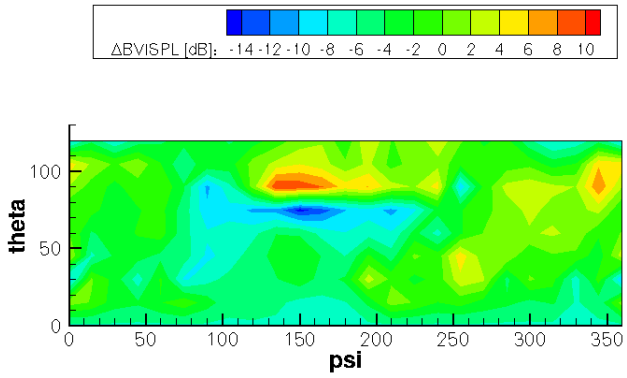

Figure 15: Technique A – B differential BVISPL at point 3 in maneuver ID8021.

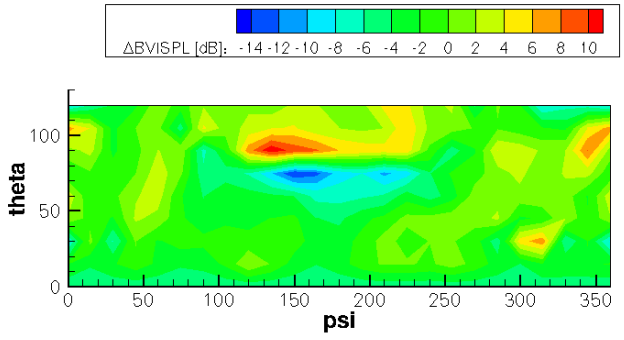

Figure 16: Technique A – C differential BVISPL at point 3 in maneuver ID8021.

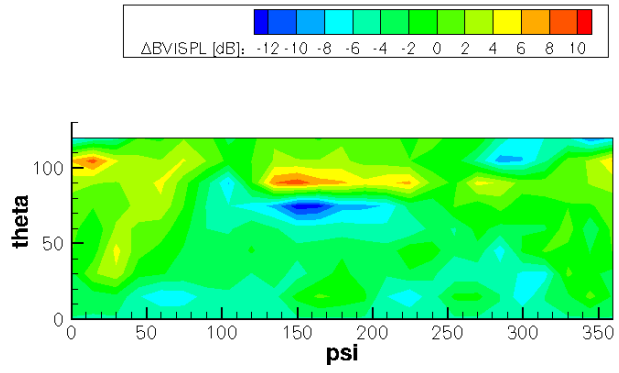

Figure 17: Technique A – B differential BVISPL at point 4 in maneuver ID8021.

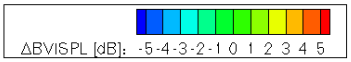

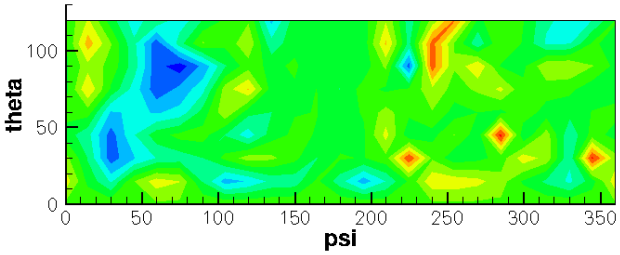

Figure 18: Technique B – C differential BVISPL at point 4 in maneuver ID8021.

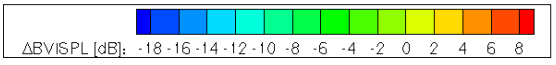

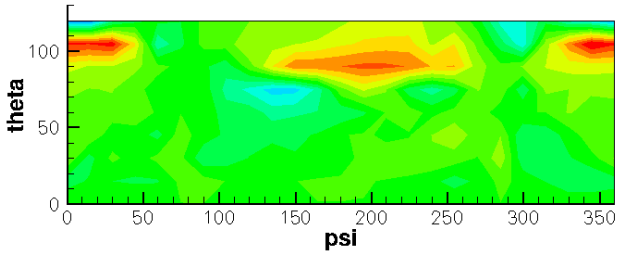

Figure 19: Technique A – B differential BVISPL at point 1 in maneuver ID8022.

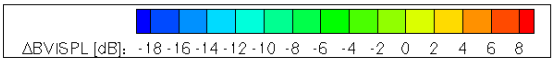

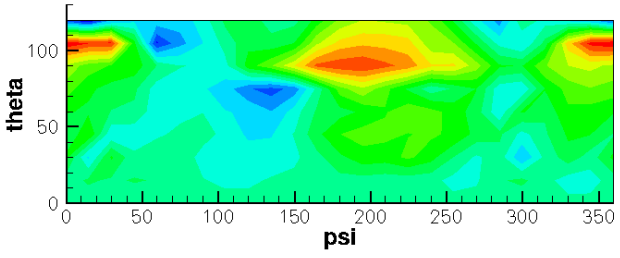

Figure 20: Technique A – C differential BVISPL at point 1 in maneuver ID8022.

quite similar, as seen in Figure 4. For the sake of conciseness, these results are not shown.

In view of the aeroacoustic results obtained for procedure ID8021, which show that the unsteady effects leading to higher discrepancies between Techniques B and C predictions are found at Point 1, two additional points of transition from uniform to decelerated flight have been examined, each from a different helicopter maneuver. Starting from the same level, steady rectilinear flight at 90 kn, procedure ID8022 is characterized by a faster deceleration to 50 kn, which are reached in 20 s, while procedure ID8023 is even faster, reaching 50 kn in 10 s. Considering the contour plots of the BVISPL, Figure 19 shows the differential of predictions from Techniques A and B, whereas Figure 20 presents the correlation between Techniques A and C, for Point 1 in procedure ID8022. With respect to the basic ma-

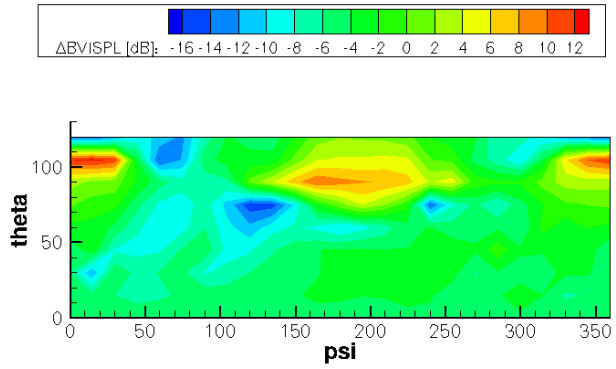

Figure 21: Technique A – B differential BVISPL at point 1 in maneuver ID8023.

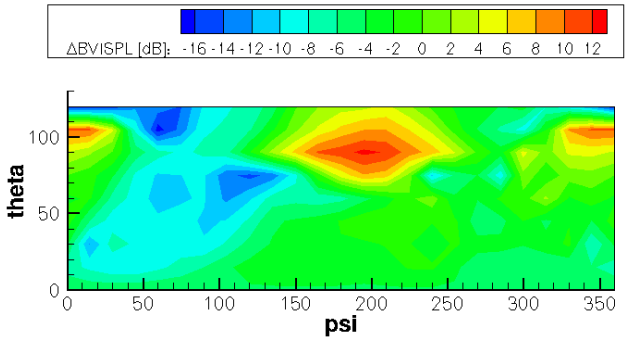

Figure 22: Technique A – C differential BVISPL at point 1 in maneuver ID8023.

neuver considered, the prediction provided by Technique B remains of similar good quality (particularly towards the polar region), whereas Technique C presents areas of larger discrepancy as compared with Technique A.

Similar considerations may be drawn observing Figures 21 and 22, that concern the correlations of Techniques B and C with Technique A for the Point 1 in procedure ID8023, where higher unsteady effects arise. Small isolated regions of high underestimation/overestimation of the acoustic signal appear, but they tend to be confined in the equatorial region. Nonetheless, Technique B results remain of good quality soon below the equatorial circle, thus confirming its suitability for application in the PAI device. In addition, the improvement in noise prediction quality moving from Technique C to B is increased with respect to what observed at Point 1 in procedures ID8021 and ID8022.

The results obtained thus far show the successful application of the complex of simulation tools described above to various unsteady flight conditions relevant to low-noise approach maneuvers. The main outcomes are related to the confirmation of a better approximation provided by Technique B, enabled by the MANOEUVRES developments concerning in-flight TPP-AOA observation and rotor state measurement, with respect to Technique C, which relies on a simplified model for TPP-AOA estimation. This demonstrates the advantages deriving from direct measurements of the main rotor blade motion. As expected, the difference between Techniques B and C grows with increasing unsteadiness. Also, the higher deviations of quasi-steady predictions with respect to fully unsteady ones are typically found in the equatorial region (about the rotor plane), while in the lower part of the hemisphere, *i.e.* the region more strictly related to ground radiated noise, the approximations are closer to the reference solution.

4 TPP-AOA observation

4.1 Framework

Within the MANOEUVRES approach, the possibility to develop a methodology for in-flight noise monitoring depends on the accurate estimation of the parameters (μ, C_T, α_{TPP}) which are used to parameterize the precalculated acoustic database employed in Technique B. Given the nature of these quantities, a direct measurement on board is unavailable. However, while an adequate estimation of the advance ratio and the thrust coefficient is possible on the grounds of the diverse measurements currently performed in flight (such as airspeed, inertial acceleration, pressure altitude, main rotor speed, etc.), the accurate TPP-AOA determination is a difficult task, given its dependence on the fuselage relative orientation with respect to airspeed and rotor TPP relative orientation with respect to the fuselage.

In order to tackle this problem, a novel method to estimate the parameters (α_{TPP}, C_T) was presented in [25]. The process starts from a set of basic measures typically available on most helicopters, augmented by a measurement of the flapping motion of the blades, in the form of the cone angle and of the 1/rev (one per rotor revolution) amplitude and phase of the flap angle. In the following, this observation method is recapitulated and applied to a basic landing maneuver, assumed as design condition. Further results assess the goodness of the proposed method with respect to off-design conditions, hence paving the way for the development of a more complete methodology for noise prediction: provided a more general database is available, the observer may enable its use by estimating the necessary parameters not only during landing, but also in more general flight conditions.

4.2 Observer structure

In order to postulate the structure of an observer for a set of desired aero-mechanical quantities based on the knowledge of an assigned set of measures, it is useful to study the relationship existing between all these variables. The equation for the main rotor flapping blade, which will be briefly recalled in this paragraph, provides a comprehensive view of such relationship, involving the variables defining the state of the helicopter from the viewpoint of flight mechanics and those characterizing the flap-wise motion of the blade. The relevant derivation process, based on the equilibrium of moment acting on the blade at its flap hinge, including hinge offset effects, is synthetically reported in [25], based on the presentation found in [42].

Assuming a flap solution composed of a constant term and a 1/rev oscillating term with its phase, the angle of flap β can be expressed in terms of the 'coning' a_0 and the longitudinal and lateral cyclic flappings a_{1_s} and b_{1_s},

$$\beta = a_0 - a_{1_s} \cos\psi - b_{1_s} \sin\psi \tag{6}$$

where ψ represents the blade azimuth. Analogously, sectional blade pitch θ at a distance r' from the flapping hinge is expressed as

$$\theta = \theta_0 + \theta_1 \frac{r'}{R} + A_1 \cos\psi + B_1 \sin\psi \tag{7}$$

in terms of the collective pitch θ_0, the lateral and longitudinal cyclic pitches A_1 and B_1, and the linear twist given by θ_1, while R is the rotor radius.

Within the blade-element momentum theory under an hypothesis of small-angles, the centrifugal, inertial, aerodynamic and weight contributions are summed and the equilibrium is imposed on their constant and cyclic components. The equilibrium relations represent a set of equations which are typically used to determine the amplitudes of the flap response (a_0, a_{1_s}, b_{1_s}) when all other parameters are known. However, here these relations are reworked to yield a set of linear equations between variables $\mathbf{s} = (\alpha_{TPP}, C_T)^T$ and $\mathbf{m} = (a_0, a_{1_s}, b_{1_s}, \theta_0, B_1)^T$ in the form given by

$$\mathbf{Q}\,\mathbf{s} = \tilde{\mathbf{T}}\,\mathbf{m} + \tilde{\mathbf{q}} \tag{8}$$

where matrices $\mathbf{Q}$ and $\tilde{\mathbf{T}}$ and vector $\tilde{\mathbf{q}}$ are given by

$$\mathbf{Q} = \begin{bmatrix} \frac{\mu^2}{2} & -\frac{1}{4} \\ 0 & 1 \end{bmatrix} \tag{9}$$

$$\tilde{\mathbf{T}} = \begin{bmatrix} 0 & \frac{1}{4} + \frac{3}{8}\mu^2 & -\frac{2eM_b}{\gamma I_b \left(1 - \frac{e}{R}\right)^2} & -\frac{2}{3}\mu & \frac{1}{4} + \frac{7}{8}\mu^2 \\ \frac{\sigma(I_b + eM_b)}{\frac{2}{3}\rho c R^4 \left(1 - \frac{e}{R}\right)} & 0 & 0 & 0 & 0 \end{bmatrix} \tag{10}$$

$$\tilde{\mathbf{q}} = -\left(\frac{1}{2}\mu\theta_1, \frac{\sigma M_b}{\frac{2}{3}\rho c R^4 \Omega^2 \left(1 - \frac{e}{R}\right)} \right)^T \tag{11}$$

These expressions have a general validity in symmetric rectilinear flight. Hence they can be assumed to describe the state of motion of the blade with an acceptable accuracy for the scope of the present analysis. Further usual hypotheses have been implicitly assumed, such as linear aerodynamics and no reverse flow region on the rotor.

The form of Equation (8) has been worked out to highlight the dependencies of the unknown variables $\mathbf{s}$ in terms of the measured variables $\mathbf{m}$, within the framework of the MANOEUVRES project. In fact, the availability of the novel rotor state measurement system allows in-flight determination of the amplitudes of the flap response (a_0, a_{1_s}, b_{1_s}) which, augmented by the control amplitudes (θ_0, B_1), retrieved from the helicopter avionics, permit the use of Equation (8) for the retrieval of (α_{TPP}, C_T).

From the definition of matrix $\mathbf{Q}$, it is clear that no singularity can be expected unless $\mu = 0$, which happens only for hover conditions. As a consequence, it is always possible to left-multiply Equation (9) by $\mathbf{Q}^{-1}$, yielding

$$\mathbf{s} = \mathbf{T}\,\mathbf{m} + \mathbf{q} \tag{12}$$

with $\mathbf{T} = \mathbf{Q}^{-1}\tilde{\mathbf{T}}$ and $\mathbf{q} = \mathbf{Q}^{-1}\tilde{\mathbf{q}}$. The previous equation clearly suggests a structure for the proposed observer. The model coefficients in $\mathbf{T}$ and $\mathbf{q}$ largely depend on constant geometrical and inertial properties of the considered helicopter rotor, such as rotor radius and solidity, flap eccentricity, and blade geometry and inertia. Furthermore, they are functions of airspeed (through advance ratio μ) and altitude (through air density ρ). As both airspeed and altitude vary during the approach maneuvers of interest, an investigation concerning the effects of such changes has been carried out and the results show that a very large variations arises in the model coefficients for even large changes in density altitude, while a much stronger dependence on airspeed is observed – as easily expected, given the impact of aerodynamics. Consequently, the model coefficients are intended as functions of the advance ratio, $\mathbf{T} = \mathbf{T}(\mu)$ and $\mathbf{q} = \mathbf{q}(\mu)$.

An important remark concerns the values of the control amplitudes (θ_0, B_1). It is possible to reduce the size of the array $\mathbf{m}$ of necessary measurements under the hypothesis of trimmed flight. Indeed, in such conditions, a relation between control amplitudes and flapping amplitudes can be assumed, permitting to consider a reduced vector

$\mathbf{m} = (a_0, a_{1_s}, b_{1_s})^T$. This may be extended to general quasi-static maneuvers without significant loss of accuracy.

Provided that all quantities explicitly reported in Equations (9)–(11) are known with sufficient accuracy, it could be possible to find the model coefficients directly, using their respective definitions. However, this approach may suffer from the effects of the many hypotheses connected to the derivation of the model, which is a simplified representation of reality.

Therefore, an alternative approach through parameter identification has been considered here to find the required model coefficients. It should be remarked that, in addition to skipping unnecessary computations of all quantities appearing in Equations (9)–(11), an approach through parameter identification allows the synthesis of a model effectively tailored to the dataset used for the identification process. Provided the identification campaign is properly planned to cover all operational conditions of interest, the assumed model structure should be able to capture the essence of the relationship between the measures and the observed signals and, if the identification algorithm is suitable for the considered problem, the accuracy of the model coefficients with respect to the testbed is usually higher than what can be obtained through purely analytic estimation, as shown in [43].

4.3 Synthesis of the observation model

In order to compute the coefficients $\left(\mathbf{T}(\mu), \mathbf{q}(\mu)\right)$ of the proposed model, an approach based on model identification has been developed, based on the procedure proposed in [43] and references therein. On account of the dependence of the observation model on μ, the coefficients can be found for an assigned value $\overline{\mu}$. In order to identify the model matrix of a linear model $\mathbf{T}(\overline{\mu})$, it is necessary to collect time samples composed of measures of the quantities to be observed $\mathbf{s}_i$ and of the measures $\mathbf{m}_i$ intended for feeding the observer. Furthermore, the identification of the coefficients of $\mathbf{q}(\overline{\mu})$ can be carried out by augmenting the array of measurements with a unitary element and performing the identification on a homogeneous system structure. To this aim, the model matrix of the homogeneous system can be defined as $\mathbf{K}(\overline{\mu}) = (\mathbf{T}(\overline{\mu}), \mathbf{q}(\overline{\mu}))$.

In practice, the samples composing the time histories of the signals measured in the simulation runs performed for identification have been distributed based on their respective airspeed values into pre-determined, non-overlapping buckets. All samples attributed to a certain airspeed bucket contribute to the identification of the model corresponding to the reference $\overline{\mu}$.

Collecting the values of $\mathbf{s}_i = (\alpha_{TPP}, C_T)_i^T$ and $\mathbf{m}_i = (a_0, a_{1_s}, b_{1_s})_i^T$ for $i = 1, \ldots, N_p$, where N_p is the number of considered samples for the assigned $\overline{\mu}_p$ value, the homogeneous model matrix $\mathbf{K}(\overline{\mu}_p)$ will be such that

$$\mathbf{S} = \mathbf{K}(\overline{\mu}_p)\ \mathbf{M} \tag{13}$$

where $\mathbf{S} = (\mathbf{s}_1, \ldots, \mathbf{s}_{N_p})$ and $\mathbf{M} = (\mathbf{m}_1, \ldots, \mathbf{m}_{N_p})$. The values of the coefficients of the model matrix for the assigned $\overline{\mu}$ value can be obtained through any suitable identification method. For the problem under analysis, a least-squares method was chosen, yielding

$$\hat{\mathbf{K}}(\overline{\mu}_p) = \mathbf{S}\mathbf{M}^T\left(\mathbf{M}\mathbf{M}^T\right)^{-1} \tag{14}$$

where the superposed hat indicates that $\hat{\mathbf{K}}$ is an estimate of $\mathbf{K}$. Once the coefficients of the model matrix are known, $\hat{\mathbf{K}}(\overline{\mu}_p)$ can be used for obtaining an online estimation of the desired quantities $\hat{\mathbf{s}}$ from a measurement of the parameters $\mathbf{m}$,

$$\hat{\mathbf{s}} = \hat{\mathbf{K}}(\overline{\mu}_p)\,\mathbf{m} \tag{15}$$

In order to use the synthesised observer in an condition where airspeed changes during the maneuver, it is necessary to preliminarily store the values of the coefficients for a suitable number of operational conditions each characterized by an appropriate $\overline{\mu}_p$ value, covering the operational airspeed envelope of the helicopter for the considered class of maneuvers. The corresponding model matrices are then interpolated online, based on the actual $\overline{\mu}$ value. In this work a linear interpolation was considered.

4.4 Preliminary numerical studies

All results presented in the following have been obtained using the RSim simulation code, a computational tool for rotorcraft flight mechanics co-developed by AgustaWestland (now Leonardo – FHD) and Politecnico di Milano in recent years, based on the general formulation reported in [44]. The simulator implements models for the flapping blade, rotor dynamic inflow and rotor wake. The considered model of helicopter represents a typical vehicle in the intermediate-weight class with fully articulated rotor and a conventional tail rotor configuration, inspired to the AW139. This model was developed at Leonardo – FHD and correlated with company proprietary data. The RSim code integrates the motion of the helicopter, which is steered by a closed-loop "maneuver tracking" technique in which collective, longitudinal and lateral pitch of the main rotor and collective pitch of the tail rotor are actuated to provide a given trajectory [40].

First, the feasibility of the proposed observer has been demonstrated by showing the quality of the identified model and, successively, by investigating the accuracy in the estimation of the TPP-AOA and the thrust coefficient, both in design and off-design conditions. The design condition for this analysis is that of a symmetric, rectilinear approach trajectory. The maneuver has been repeated for parameterized values of a set of design parameters. The starting altitude h_{in} is 3,000 ft. Values of the initial airspeed V_{in} of 30 to 50 kn with 10 kn increments have been considered. The helicopter is assumed to travel the descent trajectory in unaccelerated flight. Five glide-slope angles between 3° to 7° with 1° increments have been considered. Finally, the helicopter is stabilized in horizontal flight after reaching the final altitude h_{fin} of 500 ft. The time length of the simulations is in the order of the hundreds of seconds, the specific value depending on the airspeed and angle of descent. The data sampling frequency is 0.5 Hz. As a result of the parameterization, a total number of 150 simulations have been considered. Notwithstanding the relatively low number of simulations, the total number of samples and conditions analyzed is sufficiently high to be suitable for identification purposes.

The presence of a realistic control system simulating the action of the pilot in the control loop results in not-perfectly-constant values of the airspeed, as well as in small perturbations of other vehicle states. This circumstance can be effectively dealt with by distributing the time samples in airspeed buckets as previously mentioned. Three airspeed buckets corresponding to V_b equal to 30, 40 and 50 kn have been considered. All samples from simulations run with a weight of 94% of the reference value W_{ref}, and the coefficients of a model matrix $\hat{\mathbf{K}}\left(\overline{\mu}_b\right)$ have been computed for the value of $\overline{\mu}_b$ corresponding to each value of V_b.

In order to check the identifiability of the parameters of the proposed observer structure, once the model coefficients have been computed, it is possible to use the model matrix on the same pool of measures used for identification to perform an observation. If the model matrix that has been identified is of good quality, the 'real' (*i.e.* resulting from the simulation) and 'observed' (*i.e.* estimated through the present observation method) values of the quantity of interest should lie very close to one another, being ideally identical. In Figure 23 the result of such process for the three sampled models, corresponding to three airspeeds. The pictures show the result of the check on α_{TPP} (left) and C_T (right). On the horizontal axis the real value of the either quantity is given for each sample, whereas on the vertical axis the corresponding observation value is reported. The red solid line represents the ideal correlation between real and observed values. The quality of the observer matrix can be assessed based on the distance between the ideal line and the blue squares, each representing a sample. In this and all similar figures in this paper, only 1 sample every 100 for each simulation has been drawn, for the sake of clarity. As seen, the quality of the model is generally good on both TPP-AOA and thrust coefficient, although visibly better on the latter. This is in accordance with the model presented in Equations (9)–(11), where C_T shows an analytically simpler dependence on a smaller set of measures with respect to α_{TPP}, favoring the ease and accuracy of its observation.

An example of the time histories of the real and observed values of α_{TPP} and C_T is presented in Figure 24, while in Figure 25 the relative error for the three airspeed buckets and respective model matrices is shown for the same conditions of Figure 23. The relative errors E_{p_j} have been computed as

$$E_{p_j} = \frac{1}{N_p} \sum_{i=1}^{N_p} \frac{\sqrt{\left[\mathbf{s}_i - \hat{\mathbf{K}}\left(\overline{\mu}_p\right)\mathbf{m}_i\right]_j^2}}{[\mathbf{s}_i]_j} \tag{16}$$

with $j = 1, 2$, where $[\dots]_j$ denotes the j-th component of the vector within brackets. The left bars in Figure 25 refer to α_{TPP} and the right bars to C_T. The higher value of the error on the TPP-AOA is apparent, however both errors are considerably low, suggesting a high accuracy of the observation, which confirms the identifiability of the model according to the proposed method.

4.5 Improvements to the model structure

As the matrices in Equations (9)–(11) obtained from the theory suggest a dependence on airspeed and altitude, the actual dependence of the identified model matrices on these variables has been analyzed by considering *ad hoc* identification processes carried out first in constant-altitude, variable-speed and then in variable-altitude, constant-speed conditions. From the results detailed in [25], it is seen that the effect of changing airspeed is more marked than that of altitude, justifying the assumption that $\mathbf{K} = \mathbf{K}(\mu)$. However, given that altitude too bears some effects on the model coefficients, an extension of the observation model structure has been pursued in order to assess this dependency, including air density ρin the array of measurements, with $\mathbf{m} = (a_0, a_{1_s}, b_{1_s}, \rho)^T$. The relative observation error for a model with this augmented measurement vector was computed for the same conditions considered for the results of Section 4.4, resulting in a slight reduction in the relative error.

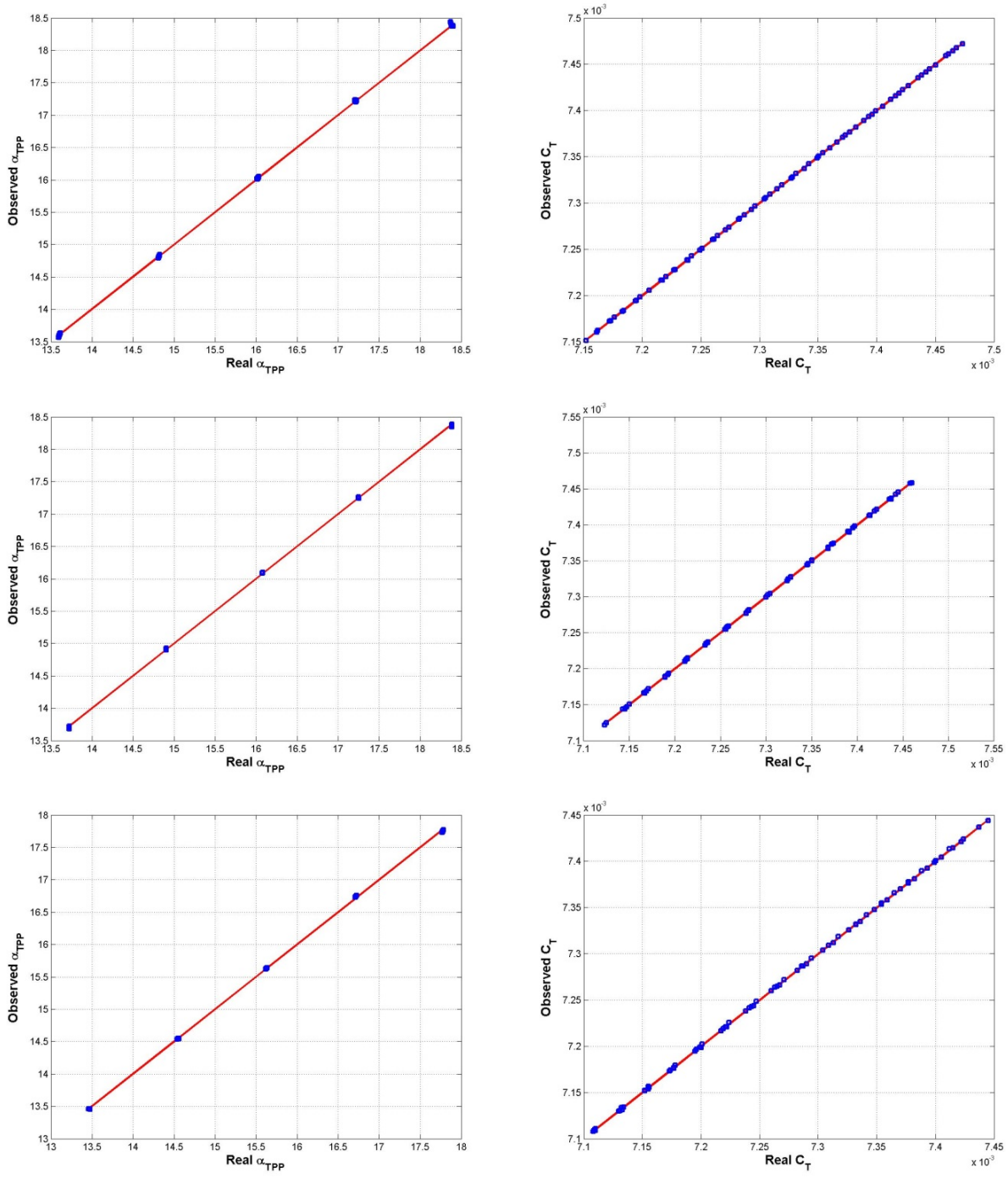

Figure 23: Model quality check for TPP-AOA (left) and thrust coefficient (right) at 30 (top), 40 (middle), and 50 (bottom) kn airspeed. Red line: ideal correlation. Blue squares: results from sampled time histories.

In a similar vein, another effect not included explicitly in the theoretical model, *i.e.* helicopter weight, has been considered. While weight can be assumed substantially constant during an approach maneuver, its effect on the model coefficients needs to be investigated due to the potential significant change of its value for different flight configurations, mainly depending on payload and fuel quantity. In this case also, a general reduction in relative error is seen with the augmented measurement vector [25].

Based on the performance advantages discussed above, the measurement array is henceforth assumed to

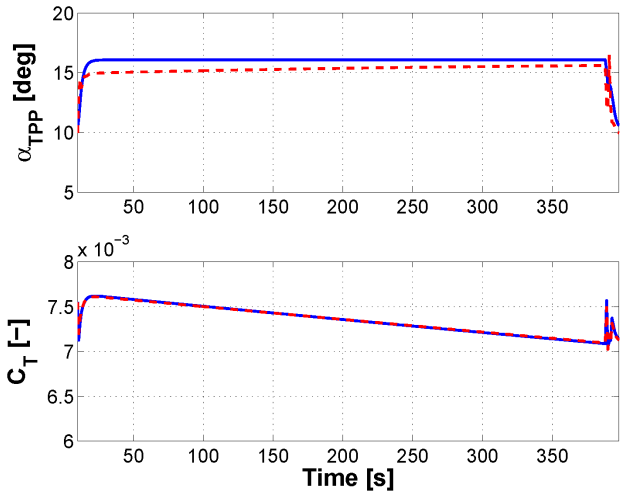

Figure 24: Time histories of real and observed values of TPP-AOA (top) and thrust coefficient (bottom) for 5° glide slope, 40 kn airspeed. Blue solid line: real values. Red dashed line: observed values.

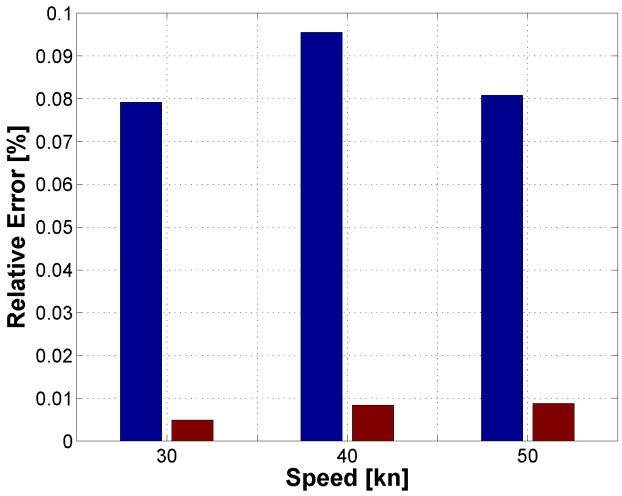

Figure 25: Average relative error for simulations at various airspeeds and glide-slope angles. Observer checked on the same samples considered for identification. Left bars: TPP-AOA, right bars: thrust coefficient.

be composed as $\mathbf{m} = (a_0, a_{1_s}, b_{1_s}, \rho, W)^T$. Figure 26 shows the relative error of the model obtained with this fully augmented array of measurements for a set of simulations where airspeed changes between 30 and 50 kn, all previously assumed glide-slope angles are considered, and multiple values of the weight are considered between 68% and 100% of W_{ref}.

4.6 Observation assessment

In order to check the accuracy provided by the proposed observation algorithm, further simulations have been performed at intermediate speeds of 35 and 45 kn, for all the weights and glide-slope angles considered in the observer synthesis process. In these new simulations, the model coefficients have been linearly interpolated for the actual value of the airspeed of each sample. The fully augmented array of measurements $\mathbf{m} = (a_0, a_{1_s}, b_{1_s}, \rho, W)^T$ has been considered. The results in Figure 27 follow the same presentation scheme used in Figure 23. It is possible to notice that the agreement between the real and observed values is good, both in terms of α_{TPP} and C_T. The relative error between observed and real values in this case is 1.91% for the TPP-AOA and 0.055% for the thrust coefficient. It can be noted that, although clearly higher than in the previous checks, the error value on both quantities remains limited, assuring good observation accuracy even when applied at airspeeds not considered for model synthesis. Furthermore, this result suggests that a relatively loose discretization with respect to airspeed as the one considered is sufficient for obtaining an acceptable level of precision.

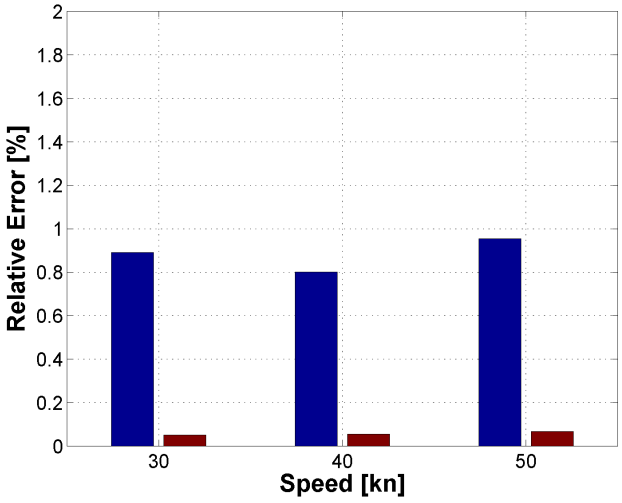

Figure 26: Average relative error for simulations at various, glide-slope angles and helicopter weights, with the measurement array augmented with air density and helicopter weight. Observer checked on the same samples considered for identification. Left bars: TPP-AOA, right bars: thrust coefficient.

A final step involved the assessment of the robustness of the observation algorithm with respect to perturbed, off-design conditions. Further simulations have been run in two scenarios departing from the one considered for identification. In the first scenario, the helicopter is sideslipping while traveling at constant airspeed and at the same values of the glide-slope angle and weight considered for identification. In the second scenario, the helicopter has

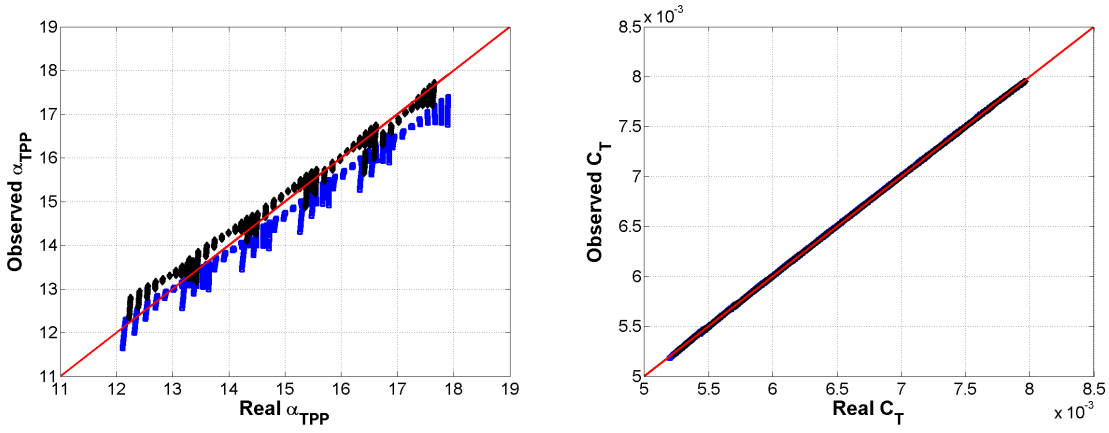

Figure 27: Observation quality check for TPP-AOA (left) and thrust coefficient (right) at 35 and 45 kn airspeed, altitudes varying between 3,000 and 500 ft, weight varying between 68% and 100% of reference value. Red line: ideal correlation. Black diamonds and blue squares: results from sampled time histories at 35 and 45 kn, respectively.

been considered to perform a decelerated descent trajectory at different constant rates of descent. The analysis discussed in [25] shows a relative error of 4.41% for the TPP-AOA and 0.363% for the thrust coefficient in the first scenario, and of 2.76% for the TPP-AOA and 0.069% for the thrust coefficient in the second. These results show that the method behaves well enough in off-design conditions to allow its practical use. However, a significant loss of accuracy has been encountered when performing simulations where the airspeed is pushed beyond the boundary considered for the scheduling of the model matrix, suggesting once more that airspeed scheduling cannot be skipped in the design of the observer.

From the discussion thus far, the proposed observation methodology appears not only feasible, but possibly capable to enable the in-flight noise estimation targeted in the MANOEUVRES project with respect to terminal maneuvers.

5 In-flight noise monitoring

5.1 Noise estimation algorithm

The starting point of the noise estimation algorithm is the database of helicopter-centered SPL hemispheres described in Section 3 calculated for an adequate range of the three mapping parameters (μ, C_T, α_{TPP}). Based on this, an interpolated SPL hemisphere can be computed for the actual values of the three mapping parameters estimated in the current flight condition.

The PAI requirements call for two different operating modes: *Emitted Noise* and *Ground Noise*. The former refers to a noise index evaluated on the surface of the SPL hemisphere, while the latter refers to a noise index evaluated at the ideal flat ground below the helicopter. In the case of the *Emitted Noise* mode, the noise index is determined by evaluating the maximum SPL values on the current interpolated hemisphere. However, for the *Ground Noise* mode, it is necessary to radiate first the SPL values from the current interpolated hemisphere to the ideal flat ground. This is achieved by a two-step process. First the SPL hemisphere, which is fixed to the helicopter body (fuselage) axes, is appropriately positioned in space taking into account the current helicopter pitch, roll and yaw attitude angles. Subsequently the SPL values are radiated to the ground and noise indexes are calculated evaluating the maximum ground pressure levels.

Wind and other atmospheric phenomena, such as fog, rain, mist, hail, wind-shear, etc., may have a significant impact on rotorcraft noise emission. However, as the present methodology is developed in view of in-flight application, the unavailability of most of the necessary atmospheric information while maneuvering inhibits to take it into account in the noise estimation algorithm. Therefore, ideal atmospheric conditions with no wind are assumed.

Multiple options have been considered for the selection of an adequate single noise index to be used for a synthetic description of the sound footprint. The values of such index should be compared with suitable threshold values. As the high-level goal of the Clean Sky GRC5 efforts is to reduce the environmental impact of rotorcraft operations, it has been decided to adopt the SPL value obtained by applying the A weighting curve [45] to produce the noise index. Since this curve is representative of the response of the human ear, it is generally adopted when

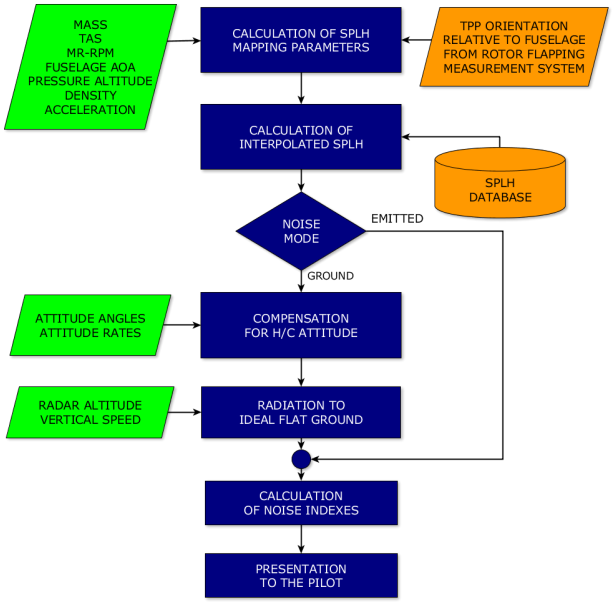

Figure 28: Flow chart of the noise estimation computational procedure.

dealing with the perception of sounds (and in particular of noise). In particular, the dBA levels thus obtained are directly comparable against the noise limits imposed by several regulations.

For the prototypal PAI application, acoustic data are provided as SPL values defined on a grid of points distributed on a hemispherical surface centred in the intersection between the main rotor axis and the TPP, assumed fixed to the helicopter body axes. The points, referred to as "microphones", are equally spaced by 15° in both latitude and longitude. In order to permit the compensation of the helicopter attitude. This grid includes thus 24 microphones on each parallel for 8 parallels with the addition of the single microphone located at the South Pole, which produces a total of 193 microphones per hemisphere. For every microphone the SPL spectrum is supplied for the first 20 multiples of the fundamental BPF at 28 Hz intervals, in the range 28–560 Hz. Since all PAI-related calculations are frequency independent, the A-weighted noise intensity has been pre-calculated for every microphone in each SPL hemisphere in the database. The radius R_H of the SPL hemisphere has been chosen as 150 m, which ensures that for any distance $R > R_H$ dipole effects can be assumed to be negligible, and the helicopter can be considered as an anisotropic monopole source.

Figure 28 shows the high-level flow chart of the developed computational procedure for in-flight noise estimation. The colour scheme adopted includes boxes with a white text on a blue background, which indicate steps of the procedure; boxes with a black text on a green background, which indicate data acquired on board from the helicopter avionic data bus; boxes with a black text on an orange background, which indicate data obtained from the outcomes of different MANOEUVRES Work Packages, namely the rotor state measurement system (WP2–3) and the SPL hemisphere database (WP1).

As the PAI requirements ask for an indication to the pilot of both the current and predicted values of the noise index, the procedure presented in Figure 28 is executed twice. On the first run, it is fed with the actual values of the input quantities (μ, C_T, α_{TPP}), producing the current noise index values. A second pass is then performed using a set of the input parameters which represent an estimate within a short-term window (*e.g.* 5 seconds) from the current time, yielding the predicted noise indexes. The following sections describe the main steps in the procedure sketched in Figure 28. Further details are provided in [26].

5.2 Calculation of the mapping parameters

The definitions of the three mapping parameters (μ, C_T, α_{TPP}) are given by

$$\mu = \frac{V}{\Omega R}\cos\alpha_{TPP} \tag{17}$$

$$C_T = \frac{T}{\rho A(\Omega R)^2} \tag{18}$$

$$\alpha_{TPP} = \alpha_F + i_M - a_{1_s} \tag{19}$$

where the latter rigorously applies to symmetric flight conditions. In these equations, V is the true airspeed (TAS), Ω the main rotor rotation speed, R the main rotor radius, T is the main rotor thrust magnitude, ρ the air density, $A = \pi R^2$ the area of the main rotor disc, α_F the fuselage angle of attack, i_M the tilt angle of the main rotor mast, a_{1_s} the longitudinal cyclic flap amplitude.

Advance ratio μ is computed first by the approximation $\cos\alpha_{TPP} \approx 1$ and retrieving the main rotor speed, from the Flight Management System (FMS) and the TAS from the Air Data Computer (ADC). Given the subsequent estimation of the TPP-AOA, this calculation can be corrected if necessary, taking into account the factor $\cos\alpha_{TPP}$.

For the computation of the thrust coefficient C_T, a simplified model of the helicopter is considered. Figure 29 shows the balance of the forces acting on the helicopter in a generic flight condition, corresponding to

$$m\mathbf{a} = \mathbf{T} + \mathbf{T}_{TR} + \mathbf{F} + \mathbf{W} \tag{20}$$

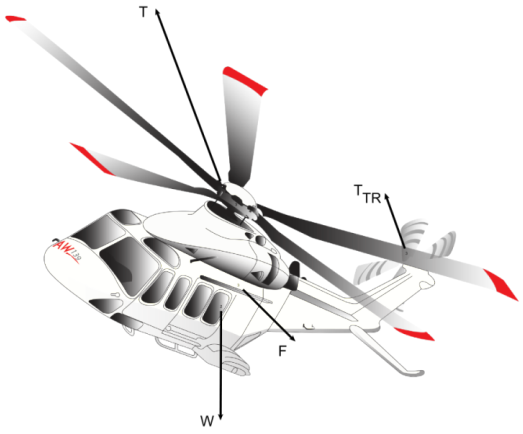

Figure 29: Balance of forces acting on the helicopter.

where m is the helicopter mass, $\mathbf{a}$ the helicopter acceleration vector, $\mathbf{T}$ the main rotor thrust vector, such that $T = \|\mathbf{T}\|$, $\mathbf{T}_{TR}$ the tail rotor thrust vector, $\mathbf{F}$ the fuselage aerodynamic force resultant vector, $\mathbf{W}$ the helicopter weight vector, such that $mg = W = \|\mathbf{W}\|$. This leads to the following expression for the thrust coefficient:

$$C_T = \frac{\|W\mathbf{n} + \mathbf{F} + \mathbf{T}_{TR}\|}{\rho A(\Omega R)^2} \tag{21}$$

where $W\mathbf{n} = (\mathbf{W} - m\mathbf{a})$ is the total mass force, or apparent weight, $\mathbf{n}$ being the load factor vector. Given appropriate models for fuselage aerodynamic forces (based on drag, sideforce and lift coefficients) and tail rotor thrust (based on a performance model, fed by current values of rotor speed and collective pitch), the above formula permits the evaluation of the thrust coefficient on the basis of geometric constant parameters of the rotor and fuselage and a number of current data retrieved by accessing the avionic data bus: main rotor speed, from the FMS; weight, also from the FMS; load factor vector, from the IRS (Inertial Reference System); air density and airspeed, from the ADC. A first approximation for C_T may be obtained by neglecting force components normal to the trajectory, and approximating the residual force with fuselage drag.

The TPP-AOA is defined in general as the angle from the main rotor TPP to the helicopter airspeed vector. As such, it can be expressed combining the orientation of the airspeed vector with respect to the helicopter fuselage body axes and the orientation of the main rotor tip path plane with respect to the fuselage. In principle, this involves the separate evaluation of the orientation of the main rotor TPP with respect to the fuselage and of the orientation of the airspeed vector with respect to the helicopter fuselage. The first problem, within the hypothesis of a definite TPP, amounts to evaluating the cyclic flapping angle components of the main rotor blades, and can be solved by resorting to the MANOEUVRES rotor state measurement system. The second problem amounts to evaluating the fuselage angle of attack and angle of sideslip, which is typically impossible through a direct measurement, unless adopting a swivelling air data boom, adequately placed outside the region interested by the main rotor wake. Today, this solution is sometimes adopted in experimental and military helicopters, while it is not considered in typical production helicopters. In absence of a direct measurement of the fuselage angles of attack and sideslip, the TPP-AOA evaluation considered in the MANOEUVRES project relies on the observation methodology presented in Section 4, which delivers an estimation of α_{TPP} and, additionally, C_T, based on rotor state measurements (a_0, a_{1_s}, b_{1_s}), possibly augmented by (ρ, W).

5.3 Noise radiation to the ground

For the *Ground Noise* PAI mode implementation, a simplified sound radiation model based on the conservation of the acoustic power has been adopted. This typically produces a slight overrating of actual noise in most of the cases, thus yielding conservative estimates, while allowing to achieve real-time performance. In any case, during normal helicopter operations, most of the quantities necessary for applying a more detailed sound propagation model are unknown, since no dedicated sensors are available on board. In this simplified propagation model, the acoustic power is invariant with distance. Therefore, the sound decay is proportional to the spherical spreading [46]. Also, this radiation model is frequency independent, so that it is possible to neglect frequency-dependent attenuation and to directly radiate the A-weighted noise intensity that has been pre-calculated for each microphone.

The radiation of the SPL values on the back-rotated hemispherical grid to the ground is sketched in Figure 30. The SPL on the ground $L_p(\theta)|_g$ corresponding to the generic microphone at latitude θ can be computed starting from the value of its value $L_p(\theta)|_H$ on the surface of the hemisphere of radius R_H as

$$L_p(\theta)|_g = L_p(\theta)|_H + A_\theta \tag{22}$$

where the attenuation A_θ is given as a function of the distance ρ_θ of the microphone to the ground along the 'acoustic ray' starting in the center of the hemisphere by

$$A_\theta = 20\log_{10}\frac{R_H}{\rho_\theta} \tag{23}$$

The shape of the grid ensures that there is no dependence of the attenuation on longitude. The distance ρ_θ can

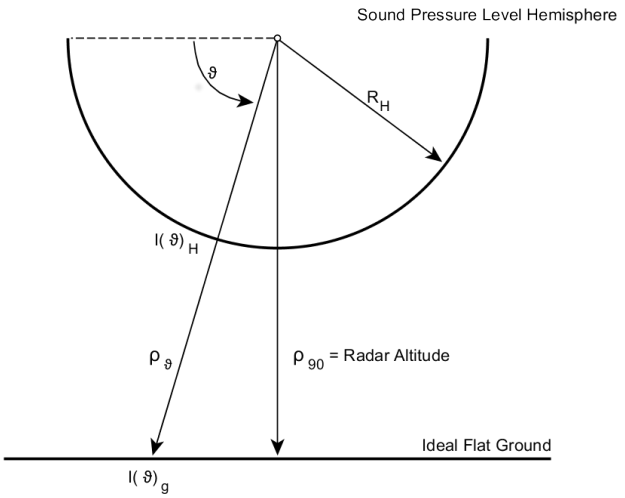

Figure 30: SPL radiation from the back-rotated hemispherical grid to the ideal flat ground.

be related to the altitude of the center of hemisphere on the terrain, represented by ρ_{90}, as

$$\rho_\theta = \frac{\rho_{90}}{\sin\theta} \tag{24}$$

therefore the final expression of attenuation results

$$A_\theta = A_{\theta_0} - 20\log_{10}\rho_{90} \tag{25}$$

where

$$A_{\theta_0} = 20\log_{10}(R_H \sin\theta) \tag{26}$$

and

$$L_p(\theta)|_g = \left(L_p(\theta)|_H + A_{\theta_0}\right) - 20\log_{10}\rho_{90} \tag{27}$$

The above expression is particularly efficient for a real time calculation, as the term within parentheses depends only on R_H and θ for each microphone, and can therefore be pre-calculated offline once and for all. The other term depends only on ρ_{90}, which is basically the current height above ground of the helicopter, as measured on board by a radar altimeter. This of course is the same for all microphones, so it needs to be calculated only once for each interpolated hemisphere.

5.4 Calculation of noise indexes

The selection of a suitable noise index has been based on the maximum value in dBA found within a given spatial domain, for both PAI operating modes. Two different measures are provided: a global one, where the noise index is simply the maximum SPL achieved on the entire grid, and a directional one, which selects the maximum SPL achieved on a specified region of the grid. In particular, five directional indexes are computed according to the subdivision of the hemispheric grid shown in Figure 31, which consists in a lower region around the South Pole and four spherical trapezoids corresponding to forward, backward, left and right of the helicopter.

Concerning predicted noise indexes, an estimation of the acoustic impact is calculated for a time window in the near future based on the current and previous trends of the helicopter kinematics. In this way, the pilot accesses information on the expected evolution of the noise index in case no specific command actions are taken. The procedure adopted for calculating the predicted noise indexes is the same, except that the mapping parameters (μ, C_T, α_{TPP}) are now estimated by extrapolating their past trend. Of course, in case of *Ground Noise* PAI mode, the prediction takes in to account the future position of the helicopter with respect to the ground.

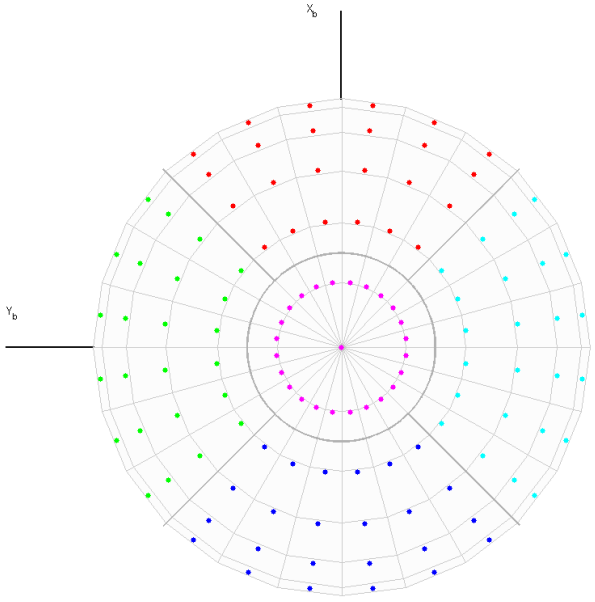

Figure 31: South Pole (bottom) view of the hemispherical microphone grid used for the Directional Indicator.

5.5 PAI design

The PAI has been conceived as a flight navigation instrument of practical and straightforward use, providing the pilot with a graphical presentation of the current and pre-

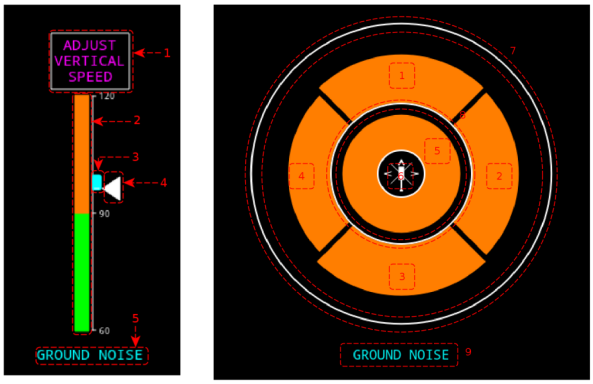

Figure 32: PAI Global Indicator (left) and Directional Indicator (right).

dicted noise index. Given that the PAI is not a primary flight navigation instrument, it has been designed to be hosted by a MFD (Multi-Function Display), with the possibility for the pilot to turn it on and off according to the situation, and to switch between its two operating modes. The *Emitted Noise* mode, which allows to appraise noise emission on a local, helicopter-centred context, can be useful to enhance crew and passenger comfort, in principle in any flight phase. The *Ground Noise* mode, taking into account radiation to the ground, is clearly the most interesting in terminal manoeuvring applications.

The PAI requirements concerning Human-Machine Interface (HMI) aspects have been defined by analysing the characteristics of modern helicopter cockpits and reviewing applicable regulations, standards and design guidelines relevant to the data presentation on aeronautical cockpit displays [47–51]. In the HMI design, all relevant elements, such as symbology, information content, advisory thresholds, guidance suggestions, enabling and disabling controls, data updating rate have been considered to promote prompt and intuitive interpretation by the pilot.

The PAI provides two different graphical presentations. The *Default Presentation* provides noise information based on the *Global Indicator*, whilst the *Full Presentation* completes the information to the pilot by showing the *Directional Indicator* alongside the *Global Indicator*. Both indicators may be used in connection with both the *Emitted Noise* and *Ground Noise* PAI operating modes.

The *Global Indicator*, shown on the left in Figure 32, refers to the global noise index and is based on a linear scale composed by two segments. The first represents admissible noise values, while the second one represents noise values exceeding a given threshold. At the side of the linear scale, a triangle-shaped pointer shows the current noise index value. This indicator also provides noise trend information in terms of a bar that, starting from the current index value, shows the expected noise index value at the end of the prediction window if no corrective action is taken by the pilot. Additionally, a corrective action can be suggested to the pilot, appearing in a dedicated advice box.

The Directional Indicator, shown on the right in Figure 32, refers to the directional noise indexes and is based on a radial scale composed by five regions: four sectors of an annulus plus a central circle. The thickness of the indication in each region is directly proportional to the current noise index relevant to that direction. Information is shown only when the noise emission index is above the currently selected threshold. In *Emitted Noise* mode, the indicated regions correspond to four lateral sectors and the lower spherical segment of the SPL hemisphere. In *Ground Noise* mode, the circular sectors display the noise index in each of the 90° azimuth sectors drawn around the ground-projected helicopter current position, while the central circle shows the noise emission index evaluated at the ground-projected helicopter current position. The *Directional Indicator* does not provide any trend information.

5.6 PAI testing

Within the MANOEUVRES project, a functional testing of the PAI through a flight simulation campaign is considered as a final demonstration. Therefore, a fully-featured PAI prototypal demonstrator has been developed and integrated in a research flight simulator available at the Helicopter System Design Department of Leonardo – FHD. The PAI hardware includes a dedicated PC, integrated in the simulator environment. The input data to the PAI algorithm are retrieved from the simulator real-time network, while the output is directly fed to the cockpit MFD.

Figure 33 shows the software architecture adopted for the PAI demonstrator. The whole functionality has been split among four co-operating tasks, communicating via TCP/IP sockets. The Data Source Task takes care to retrieve all necessary data from the Flight Simulator network (boxes with green background), to calculate current and predicted values of the three mapping parameters and to feed all information to the Noise Index Task. The latter is in charge to (i) generate the current and predicted interpolated SPL hemisphere, starting from data available in the aeroacoustic database, (ii) compensate for helicopter attitude, (iii) when in *Ground Noise* mode, radiate to the ground and (iv) pass the set of current and predicted noise index values to the Pilot Display Task, dedicated to symbols generation and display management. The Manage-

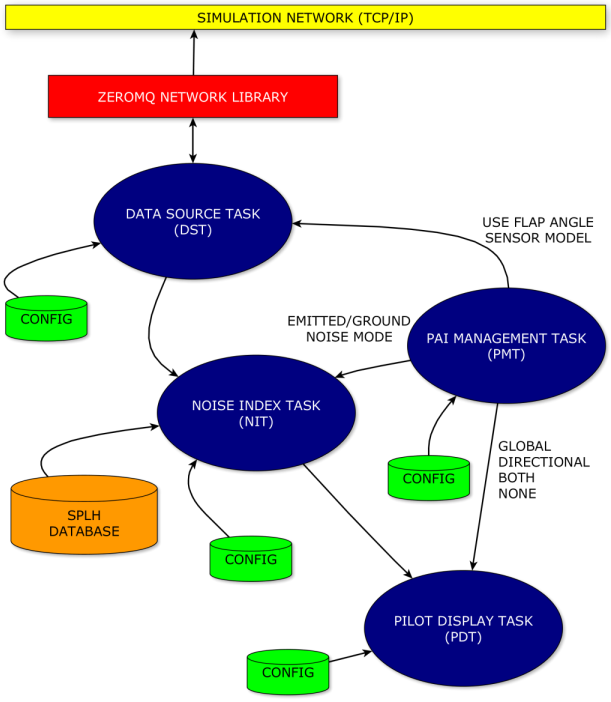

Figure 33: PAI Demonstrator software architecture.

ment Task, as the name implies, is in charge of managing the complete operation. Initial testing, demonstrated the complete functionality of the PAI integration on the Leonardo – FHD Flight Simulation facility. The final PAI demonstration shall involve professional test pilots that will assess the PAI suitability in a number of simulated terminal trajectories.

6 Conclusions

This paper provides a comprehensive view of a multidisciplinary effort aimed at developing a methodology for in-flight monitoring of the emitted noise in view of its integration on board production rotorcraft vehicles. Towards this goal, in-depth studies of the helicopter aeroacoustic footprint during maneuvering flight were devised, involving quasi-steady and fully unsteady approaches. The study performed to date has shown the capabilities of a quasi-steady approach based on pre-calculated SPL distributions in capturing unsteady noise effects, especially if invigorated by an accurate estimation of the main rotor TPP-AOA. Further planned work includes the correlation of the noise predictions with experimental data, as well as the assessment of their sensitivity with respect to perturbations in the nominal trajectory. A methodology for the estimation of the main rotor TPP-AOA has been developed to overcome the difficulty posed by the unavailability of a direct measurement of the fuselage angle of attack. This methodology consists in an observation based on model identification techniques, where an appropriate model is linearly scheduled with respect to airspeed, relying on a structure inspired by classical results stemming from the flapping blade equilibrium equation and improved on the basis of empirical evidence. The method, which may be further developed and optimized, also determines the thrust coefficient and represents a promising candidate for integration in a real-time noise estimation algorithm to be run on board. The new PAI cockpit instrument has been completely designed and its prototypal demonstrator is currently being tested within a sophisticated flight simulation environment to assess, and possibly optimize, its functional characteristics and potential relevance in aiding the pilot to perform low-noise terminal procedures. The PAI software includes a noise estimation algorithm which employs the quasi-steady aeroacoustic estimation approach and the TPP-AOA observation method to synthesize condensed noise information for cockpit presentation through a specifically developed graphical interface.

The accuracy of the proposed in-flight acoustic estimation methodology strongly relies on the availability of accurate measurements of the main rotor blade motion. This will be accomplished by means of a new contactless rotor state measurement system currently in its final development phase. The design, testing and on board integration of this system, along with the investigation on unsteady rotorcraft aeroacoustics and PAI design and development, is a major goal of the Clean Sky GRC MANOEUVRES project. This started in October, 2013, for a duration of 24 months, with an extension of further 8 months currently being implemented. Of the 4 technical Work Packages, WP1 (acoustic prediction), WP3 (rotor state measurement system development) and WP4 (in-flight noise monitoring) are currently in their final stage of development, enjoying strong co-operation with Leonardo–FHD.

Acknowledgement: The research has been partially funded by the Clean Sky Joint Undertaking Programme under Grant Agreement N. 620068. The authors acknowledge the cooperation of Emanuele Zappa, Marco Lovera, Simone Panza and Federico Rossi (Politecnico di Milano), Jacopo Serafini (Università di Roma Tre), Potito Cordisco, Edoardo Vigoni and Mauro Terraneo (Vicoter), Riccardo Grassetti (Logic), Attilio Colombo, Domenico Leonello and Enrico Paolone (Leonardo – FHD).

References

[1] Sim B. W., Beasman T., Schmitz F. H., Gopalan G., In-flight blade-vortex interaction (BVI) noise measurements using a boom-mounted microphone array, American Helicopter Society International 60th Annual Forum, Baltimore, MD, USA, June, 2004.

[2] Ishii H., Gomi H., Okuno Y., Helicopter flight tests for BVI noise measurement using an on-board external microphone, Technical Report, American Institute of Aeronautics and Astronautics, 2005–6119, Reston, VA, USA, 2005.

[3] Chen H. N., Brentner K. S., Shirey J. S., Horn J. F., Ananthan S., Leishman G., Study of the aerodynamics and acoustics of super-BVI, American Helicopter Society International 62nd Annual Forum, Phoenix, AZ, USA, 2006.

[4] Schmitz F. H., Greenwood E., Sickenberger R. D., Gopalan G., Conner D., Moralez E., Sim B. W., Tucker G., Decker W. A., Measurement and characterization of helicopter noise in steady-state and maneuvering flight, American Helicopter Society International 63rd Annual Forum, Virginia Beach, VA, USA, 2007.

[5] Brentner K. S., Jones H. E., Noise prediction for maneuvering rotorcraft, 6th AIAA/CAES Aeroacoustics Conference, Lahaina, HI, USA, 2000.

[6] Janakiram R. D., Khan H., Prediction and validation of helicopter descent flyover noise, American Helicopter Society International 56th Annual Forum, Virginia Beach, VA, USA, 2000.

[7] Brentner K. S., Brès G. A., Perez G., Jones H. E., Toward a better understanding of maneuvering rotorcraft noise, American Helicopter Society International 58th Annual Forum, Montreal, Canada, 2002.

[8] Brès G. A., Brentner K. S., Perez G., Jones H. E., Maneuvering rotorcraft noise prediction, *Journal of Sound and Vibration*, Vol. 39, 2003.

[9] Brooks T. F., Booth E. R., Jolly J. R., Yeager W. T., Wilbur M. L., Reduction of blade-vortex interaction noise using higher harmonic pitch control, NASA Technical Memorandum 101624, NASA Langley Research Center, Hampton, VA, USA 1989.

[10] Beaumier P., Prieur J., Rahier G., Spiegel P., Demargne A., Tung C., Gallman J. M., Yu Y. H., Kube R., Van der Wall B. G., Schultz K. J., Splettstoesser W. R., Brooks T. F., Burley C. L., Boyd D. D., Effect of higher harmonic control on helicopter rotor blade-vortex interaction noise: prediction and initial validation, 75th Fluid Dynamics Symposium, Berlin, Germany, 1994.

[11] Chen H. N., Brenter K. S., Anantham S., Leishman J. G., A computational study of helicopter rotor wakes and noise generated during transient maneuvers, American Helicopter Society International 61st Annual Forum, Grapevine, TX, USA, 2005.

[12] Le Duc A., Spiegel P., Guntzer F., Lummer M., Götz J. , Buchholz H., Simulation of complete helicopter noise in maneuver flight using aeroacoustic flight test database, American Helicopter Society International 64th Annual Forum, Montreal, Canada, 2008.

[13] Gennaretti M., Serafini J., Molica Colella M., Bernardini G., Simulation of helicopter noise in maneuvering flight, 40th European Rotorcraft Forum ERF 2014, Southampton, UK, 2014.

[14] Bernardini G., Anobile A., Serafini J., Hartjes S., Gennaretti M., Methodologies for helicopter noise footprint prediction in manoeuvring flights, 22nd International Conference on Sound and Vibration, Firenze, Italy, 2015.

[15] Gennaretti M., Serafini J., Bernardini G., Castorrini A., De Matteis G., Avanzini G., Numerical characterization of helicopter noise hemispheres, *Aerospace Science and Technology,* Vol. 52, pp. 18-28, 2016..

[16] Clean Sky Joint Undertaking, Call SP1-JTI-CS-2013-01, Call text, January 2013.

[17] Trainelli L., Rolando A., Zappa E., Manzoni S., Lovera M., Gennaretti M., Bernardini G., Cordisco P., Terraneo M., Vigoni E., Grassetti R., MANOEUVRES – An effort towards quieter, reliable rotorcraft terminal procedures. Greener Aviation Conference 2014: Clean Sky breakthroughs and worldwide status, Brussels, Belgium, 2014.

[18] Trainelli L., Lovera M., Rolando A., Zappa E., Gennaretti M., Cordisco P., Grassetti R., Redaelli M., Project MANOEUVRES – Towards real-time noise monitoring and enhanced rotorcraft handling based on rotor state measurements, 41st European Rotorcraft Forum ERF2015, Munich, Germany, 2015.

[19] Colombo A., Locatelli A., Measuring blade angular motions: A kinematical approach, 30th European Rotorcraft Forum ERF 2004, Marseilles, France, 2004.

[20] Cigada A., Colombo A., Cordisco P., Ferrario A., Grassetti R., Manzoni S., Redaelli M., Rolando A., Terraneo M., Trainelli L., Vigoni E., Zappa E., Contactless Rotor Flapping Sensor Design, Implementation and Testing, American Helicopter Society International 72nd Annual Forum, West Palm Beach, FL, USA, 2016.

[21] Panza S., Lovera M., Rotor state feedback in helicopter flight control: robustness and fault tolerance, IEEE Multi-Conference on Systems and Control, Antibes/Nice, France, 2014.

[22] Panza S., Lovera M., Rotor state feedback in the design of rotorcraft attitude control laws, in Bordeneuve-Guibé J., Drouin A., Roos C. (eds.), *Advances in Aerospace Guidance, Navigation and Control*, Springer, 2015.

[23] Panza S., Bergamasco M., Viganò L., Lovera M., Rotor State Feedback in Rotorcraft Attitude Control, 41st European Rotorcraft Forum ERF 2015, Munich, Germany, 2015.

[24] Gennaretti M., Bernardini G., Anobile A., Serafini J., Trainelli L., Rolando A., Scandroglio A., Riviello L., Acoustic prediction of helicopter unsteady manoeuvres, 41st European Rotorcraft Forum ERF 2015, Munich, Germany, 2015.

[25] Trainelli L., Riboldi C. E. D., Bucari M., Observing the Angle of Attack of the Tip Path Plane from Rotor Blade Measurements, 41st European Rotorcraft Forum ERF 2015, Munich, Germany, 2015.

[26] Rolando A., Rossi F., Riboldi C. E. D., Trainelli L., Grassetti R., Leonello D., Redaelli M., The Pilot Acoustic Indicator: a novel cockpit instrument for the greener helicopter, 41st European Rotorcraft Forum ERF 2015, Munich, Germany, 2015.

[27] Conner D. A., Page J. A., A Tool for Low Noise Procedures Design and Community Noise Impact Assessment: The Rotorcraft Noise Model (RNM), Heli Japan 2002, Tochigi, Japan, 2002.

[28] Le Duc A., Spiegel P., Guntzer F., Kummer M., Götz J., Modelling of Helicopter Noise in Arbitrary Maneuver Flight Using Aeroacoustic Database, 9th Onera-DLR Aerospace Symposium (ODAS 2008), Châtillon, France, 2008.

[29] Hartjes S., Buys Y., Visser H. D., Pavel M. D., Gennaretti M., Bernardini G., Arntzen M., Optimization of Rotorcraft Noise Abatement Trajectories, Internoise 2012/ASME NCAD meeting, New York City, USA, 2012.

[30] Greenwood E., Schmitz F. H., Sickenberger R. D., A semi-empirical noise modeling method for helicopter maneuvering flight operations, American Helicopter Society International

68th Annual Forum, Fort Worth, TX, 2012.
[31] Greenwood E., Rau R., May B., Hobbs C., A maneuvering flight noise model for helicopter mission planning, American Helicopter Society International 71st Annual Forum, Virginia Beach, VA, 2015.
[32] Gopalan G., Schmitz F. H., A Sensitivity analysis of the quasi-static acoustic mapping of helicopter Blade-Vortex Interaction (BVI) noise during slowly maneuvering flight, 9th AIAA/CEAS Aeroacoustics Conference, Hilton Head, SC, May 2003.
[33] Brentner K. S., Jones H. E., Noise Prediction for Maneuvering Rotorcraft, AIAA Paper 2000–2031, 6th AIAA/CEAS Aeroacoustics Conference, Lahaina, Hawaii, 2000.
[34] Farassat F., Derivation of Formulations 1 and 1A of Farassat, NASA TM 214853, 2007.
[35] Brès G. A., Brentner K. S., Maneuvering Rotorcraft Noise Prediction, *Journal of Sound and Vibration*, Vol. 275, 2004, pp. 719–738.
[36] Johnson W., *Comprehensive Analytical Model of Rotorcraft Aerodynamics and Dynamics*, Vol. I - VII, Johnson Aeronautics, 1998.
[37] Sarathy S., Higman J., Development and validation of the OH-58D Kiowa Warrior high fidelity flight simulation model,American Helicopter Society International 50th Annual Forum, Washington, DC, 1994.
[38] Padfield G. D., White M. D., Flight simulation in academia - HELIFLIGHT in its first year of operation, The Challenge of Realistic Rotorcraft Simulation RAeS Conference, London, 2001.
[39] Gassaway B., Strope K., Cicolani L., Lusardi J., He C., Robinson D., Predictive Capabilities of a UH-60 FLIGHTLAB Model with an External Sling Load, American Helicopter Society International 62nd Annual Forum, 2006.
[40] Serr C. et al., Improved methodology for take-off and landing operational procedures - The RESPECT programme, 25th European Rotorcraft Forum ERF1999, Rome, Italy, 1999.
[41] Quackenbush T. R., Wachspress D. A., Boschitsch A. H., Rotor aerodynamic loads computation using a constant vorticity contour free wake model, *Journal of Aircraft*, Vol. 32, No. 5, 1995, pp. 911-920.
[42] Prouty R. W., *Helicopter Performance, Stability and Control*, Robert E. Krieger Publishing Company, 1990.
[43] Bottasso C. L., Riboldi C. E. D., Estimation of wind misalignment and vertical shear from blade loads, *Renewable Energy*, Vol. 26, 2014, pp. 293–302.
[44] Padfield G., *Helicopter Flight Dynamics*, Blackwell Science, 1996.
[45] ANSI S1 Rev. 4 – Specification for sound level meters, American National Standards Institute, 1983.
[46] Marburg S., Nolte B., *Computational Acoustics of Noise Propagation in Fluids – Finite and Boundary Element Methods*, Springer, 2009.
[47] Advisory Circular 25-11B: Electronic Flight Displays, Federal Aviation Administration, 2014.
[48] Advisory Circular 25.1302-1: Installed Systems and Equipment for Use by the Flightcrew, Federal Aviation Administration, 2013.
[49] Certification of Transport Category Rotorcraft, Federal Aviation Administration, 2013.
[50] Standard ARP4032B: Human Engineering Considerations in the Application of Color to Electronic Aircraft Displays, SAE, 2013.
[51] Standard ARP5364: Human Factor Considerations in the Design of Multifunction Display Systems for Civil Aircraft, SAE, 2003.